The Cryosphere Discuss., https://doi.org/10.5194/tc-2019-30
Manuscript under review for journal The Cryosphere
Discussion started: 18 February 2019

The Cryosphere Discussions
Open Access
EGU

Multi-year Evaluation of Airborne Geodetic Surveys to Estimate Seasonal Mass Balance, Columbia and Rocky Mountains, Canada

Ben M. Pelto[1], Brian Menounos[1], Shawn J. Marshall[2]

[1]Natural Resources and Environmental Studies Institute and Geography Program, University of Northern British Columbia, Prince George, V2N 4Z9, Canada
[2]Department of Geography, University of Calgary, Calgary, T2N 1N4, Canada

Correspondence to: Ben M. Pelto (pelto@unbc.ca)

Abstract. Seasonal measurements of glacier mass balance provide insight into the relation between climate forcing and glacier change. To evaluate the feasibility of using remotely-sensed methods to assess seasonal balance we completed tandem airborne laser scanning surveys (ALS) and field-based glaciological measurements over a four-year period for six alpine glaciers that lie in Columbia and Rocky Mountains, near the headwaters of the Columbia River, British Columbia, Canada. We calculated annual geodetic balance using co-registered late-summer digital elevation models (DEMs), and distributed estimates of density based on surface classification of ice, snow and firn surfaces. Winter balance was derived using co-registered late-summer and spring DEMs, and density measurements from regional snow course observations and our glaciological measurements. Geodetic summer balance was calculated as the difference between winter and annual balance. Winter mass balance from our glaciological observations averaged 1.95 ± 0.09 m w.e., 4% greater than those derived from geodetic surveys. Average glaciological summer and annual balance were also 4% greater than our geodetic estimates. We find that distributing snow, firn and ice density based on surface classification has a greater influence on geodetic annual mass change than the density values themselves. Our results demonstrate that accurate assessments of seasonal mass change can be produced using airborne ALS over a series of glaciers spanning several mountain ranges. Such agreement over multiple seasons, years, and glaciers demonstrates the ability of high-resolution geodetic methods to increase the number of glaciers where seasonal mass balance can be reliably measured.

1 Introduction

Glacier mass balance is a function of accumulation and ablation processes, responding directly to meteorological forcing at timescales of a season or more (Oerlemans et al., 1998). Mass balance observations help address research about changes of glacier runoff (Jost et al., 2012; Ragettli et al., 2016; Stahl and Moore, 2006), contributions of glacier mass loss to sea level rise (Bahr et al., 2009; Huss and Hock, 2015; Radić and Hock, 2011), and the response of glaciers to climate change (Clarke et al., 2015). Annual mass balance is the sum of accumulation and ablation throughout the balance year. Measurement of seasonal mass change provides one method to assess the importance of meteorological drivers of glacier nourishment and melt.

Unfortunately, seasonal balance is logistically and financially difficult, and these challenges lead to few seasonal mass balance records at the global scale (Ohmura, 2011). Currently, seasonal balance measurements for western Canadian glaciers are not publicly available (WGMS, 2017). Seasonal snowpack forms a critical component of glacier mass balance (Machguth et al., 2006). Knowledge of the high elevation snowpack and its change through time is limited or non-existent for most alpine regions (Barnett et al., 2005; Hamlet et al., 2005), including most glaciers within the Canadian Columbia River Basin (Brahney et al., 2017). A better understanding of the seasonal snowpack and its changes is needed to ascertain whether it is changing and whether and will offset or exacerbate increased ablation.

Several recent studies have used geodetic methods to measure seasonal snow depth on glaciers (Dadic et al., 2010; Helfricht et al., 2014; Machguth et al., 2006; McGrath et al., 2015; Sold et al., 2014) and to measure seasonal mass balance (Belart et al., 2017; Sold et al., 2013). Geodetic methods offer the ability to greatly expand the number of glaciers over which these measurements can occur (Berthier et al., 2014; Nolan et al., 2015). The primary objective of our study is to evaluate the reliability of geodetic surveys for estimation of seasonal mass change of temperate glaciers over multiple years.

1.1 Study Area

1.1.1 Columbia Mountains

The transboundary Columbia River Basin (668,000 km^2) spans seven U.S. states and British Columbia (BC), Canada. The Canadian portion of the Basin represents 15% of the watershed's total area, yet provides between 30-40% of its total runoff, largely due to the presence of mountainous terrain with high amounts of orographic precipitation and extensive glacial cover (Cohen et al., 2000; Hamlet and Lettenmaier, 1999). There are 2,200 glaciers covering 1,760 km^2 in the Columbia Mountains (Bolch et al., 2010); these glaciers primarily exist within the Cariboo, Monashee, Selkirk, and Purcell ranges, with the highest elevations rising to over 3,000 m above sea level (asl).

The climate of the Columbia Mountains is transitional between maritime and continental (Demarchi, 2011), with a strong maritime influence (Hägeli and McClung, 2003). Monthly average temperatures in the Canadian CRB (elevation range from 420 to 3700 m asl) range from -9.2˚C in January to 13.3˚C in July (Najafi et al., 2017; Schnorbus et al., 2014). General circulation is dominated by westerly flow, which brings consistent Pacific moisture, particularly in the winter months. Approximately 65% of annual precipitation falls as snow, with snowfall possible throughout the year (Schnorbus et al., 2014). The snow accumulation season in both the Columbia and Canadian Rocky Mountains extends from October to May. The summer melt season runs from May through September.

1.1.2 Rocky Mountains

The southern Canadian Rockies are located east from the Columbia Mountains across the Rocky Mountain Trench and are home to 1090 glaciers covering 1350 km^2 (Bolch et al., 2010).

The eastern slopes of the Canadian Rocky Mountains experience a continental climate with mild summers and cold winters. However, winter precipitation along the continental divide is greatly influenced by moist Pacific air masses, with persistent westerly flow driving orographic uplift on the western flanks of the Rocky Mountains (Sinclair and Marshall, 2009). This combination of continental and maritime influences fosters extensive glaciation along the continental divide in the Canadian Rockies, with glaciers at elevations from 2200 to 3500 m asl on the eastern slopes. The Canadian Rockies are drier, clearer, and colder in winter than the Columbia Mountains.

2 Data and Methods

2.1 Study Sites

Over the period 2014-2018 we measured seasonal mass balance of six alpine glaciers (Figure 1, Table 1): (1) Zillmer Glacier (5.4 km^2) in the Cariboo Mountains, (2) Nordic Glacier (3.4 km^2) in the Selkirk Mountains, (3) Illecillewaet Glacier (7.7 km^2) in the Selkirk Mountains, (4) Conrad Glacier (11.5 km^2) in the Purcell Mountains, (5) Haig Glacier (2.6 km^2), which straddles the continental divide in the Rocky Mountains, and (6) Kokanee Glacier (1.8 km^2) in the Purcell Mountains.

2.2 Geodetic Mass Balance

We performed repeat fixed-wing ALS surveys from late-summer 2014 to late-summer 2016 (Table 2) using a Riegl VQ-580 infrared (1024 micron) laser scanner with dedicated Applanix POS AV Global Navigation Satellite System (GNSS) Inertial Measurement Unit (IMU). Later surveys used the same GNSS IMU and a Riegl VQ-780 infrared (1024 micron) laser scanner. The VQ-580 was typically flown at a height of 500 m above the terrain, whereas the VQ-780 was flown at 2600-2700 m above the terrain to enable wider swatch widths compared to the VQ-580. We planned the airborne surveys to yield return point densities that averaged 1-2 laser shots m^{-2} with an effective sampling diameter of 10-20 cm per laser shot.

2.2.1 ALS Post-Processing

Post-processing of the ALS survey flight trajectory data used the PosPac Mobile Mapping Suite (Applanix), with Trimble CenterPoint RTX with vertical and horizontal positional uncertainties that were typically better than ±15 cm (1σ). We cleaned point clouds and exported finished LAS files into LAStools (https://rapidlasso.com/lastools/) where we created 1-m digital elevation models (DEM) from each survey. We co-registered all DEMs following the method detailed in Nuth and Kääb (2011). For late-summer surveys, one master DEM was chosen and all other late-summer DEMs were co-registered to that DEM for stable surfaces only. Stable surfaces were identified in satellite imagery and excluded forests, lakes and ice- and snow-covered areas, which were all masked out. For winter DEMs, the previous late-summer DEM was used as the master DEM to mitigate against any surface height changes in areas defined as stable terrain, due to processes such as rockfall or vegetation height change. During the spring surveys, there was little to no snow-free terrain, except rocky features with extreme

The Cryosphere Discuss., https://doi.org/10.5194/tc-2019-30
Manuscript under review for journal The Cryosphere
Discussion started: 18 February 2019

slopes which are not used in the co-registration (slope >40˚ excluded). We thus did not apply any vertical shift during co-registration of winter DEMs.

We utilized satellite imagery from Landsat 7 and 8, Sentinel-2, and Planet Scope at 30, 10, and 3-to-5 m resolution respectively (Bevington et al., 2018), to guide surface classification used to co-register DEMs and calculate geodetic mass change. We selected the latest snow-free imagery from September or late-August, and used a band-ratio and threshold method (Kääb, 2005) to classify areas of snow, firn, and ice. In some cases, we manually corrected surface maps where our automated methods failed to differentiate between firn and snow surfaces.

To calculate annual mass change (B_a), we (1) difference two DEMs to create a height change DEM (ΔDEM), (2) determine the mean difference between the two DEMs in stable terrain ($Bias_{\Delta h}$, Table 3) to bias-correct the observed height change by any systematic elevation difference between the DEMs after co-registration, (3) derive a mask based on surface classification of ice, firn and snow from satellite imagery (Figure S1), then (4) apply the density of each respective surface type (Table 4), to the ΔDEM to calculate mass balance.

For late-summer DEMs, stable terrain generally covered 10-20 km^2, providing enough area for bias (Figure S2) and uncertainty assessment. To calculate uncertainty in ALS-derived height change, we also account for spatial correlation as assessed over stable terrain based on semi-variogram analysis (Figure S3) as described in Rolstad et al. (2009). We chose not to use Digital Terrain Models (DTMs), which represent gridded elevation based on last returns from the laser scanner, since our gridding algorithms employed in LAStools filled crevasses and did not preserve sharp ridges that aided in co-registration of the DEMs.

Annual glacier mass balance is defined as the sum of accumulation and ablation throughout the balance year (Cuffey and Paterson, 2010), which can be expressed as the sum of winter and summer balance:

$$B_a = B_w + B_s \quad (1)$$

For geodetic and glaciological mass balance, we measure winter and annual balance, and use the difference between them as summer balance (Cuffey and Paterson, 2010):

$$B_s = B_a - B_w \quad (2)$$

To calculate geodetic winter balance (B_{w_geod}), we created a ΔDEM from the previous late-summer DEM, and the given spring DEM of interest, and then applied spring snow density (Table 4). We did not independently estimate B_{s_geod} because of the added uncertainty of partitioning elevation change due to melt or compaction of snow/firn surfaces.

2.2.2 Density Estimates

While ALS provides an accurate estimate of snow depth with vertical uncertainties of ±0.1–0.3 m (Abermann et al., 2010; Bollmann et al., 2011; Joerg et al., 2012), it provides no information regarding snow density. We use snow course measurements available from the British Columbia River Forecast Center (BCRFC) (Najafi et al., 2017; Schnorbus et al., 2014) as independent data to estimate spring snow density, and compare this with our measured glaciological snow densities. We use these BCRFC data to evaluate whether reliable estimates of snow density can be obtained for regions where no snow observations over glaciers exist. The mean date of our spring field visits was May 1st (Table 2), so we chose May 1st snow

course data (n = 10,169) to derive a relation between SWE (kg m^{-2}) and snow depth (m) (Figure 2). The linear relation (regression fit) yields a slope of 470 ± 70 kg m^{-3} (r^2 = 0.97), which we use as the average May 1st snow density which we applied for our geodetic B_w calculations. For Haig Glacier, we chose only snow course measurements from the Rocky Mountains for a linear relation yielding 440 ± 50 kg m^{-3} (n = 629). The estimated uncertainty in bulk snow density (±70 and ±50 kg m^{-3}) represents the standard deviation (σ) of the snow course data. For our glaciological density-informed B_{w_geod}, we use the observed glacier-wide snow density (Table S1) and a linear regression of density versus day and used the slope (3.0 kg m^{-3} day^{-1}, r^2 = 0.43) and days between the survey and the observations to adjust for change in snow density (Figure 3). The lack of an altitudinal trend in snow density observed on many glaciers (Fausto et al., 2018; McGrath et al., 2015, 2018; Sold et al., 2016) and those of this study, coupled with the absence of high-elevation snow density measurements and the annual variability of snow density evolution, required the use of a single value for spring snow density.

Regional observations of late-summer snow density are consistent (Table 5); ranging from 530-630 kg m^{-3} for glaciers across the Pacific Northwest (Table 5). This is expected for temperate, mid-latitude glaciers, where snow densities range from the "critical density" of about 550 kg m^{-3} (Benson, 1962; Herron and Langway, 1980) to around 600 kg m^{-3} depending upon regional climatology. Since we independently evaluate glaciological vs. geodetic estimates of mass change, we compare application of our late-summer glaciological snow density measurements to calculate net balance with estimates based on the average of typical observations from four regional sources (590 ± 60 kg m^{-3}; Table 5), to test the impact of uncertainties of up to 10% in this parameter. Firn density has not been reported for the study area, so we estimate 700 ± 100 kg m^{-3} for multi-year firn based on observations in the Alps (Ambach et al., 1966). This is also consistent with our firn core measurements for firn two or more years old (Table S2; average density of 703 ± 65 kg m^{-3}, n=4). Measurements of one-year-old firn averaged 619 ± 47 kg m^{-3} (n=8). Given the sustained mass loss of Pacific Northwest glaciers (Bolch et al., 2010; Menounos et al., 2018; Pelto, 2006), exposed firn is generally more than one year old, and we apply an uncertainty of two times the σ of our multi-year firn core observations (±15%), which captures the range of observed firn densities (664-776 kg m^{-3}). We use an ice density of 910 ± 10 kg m^{-3} (Clarke et al., 2013). After performing a pixel-based surface classification for each late-summer, we used these classification masks to assign a density (Table 4) to each pixel (snow/firn/ice).

2.2.3 Firn Densification

Firn densification (Belart et al., 2017; Sold et al., 2013) can be modeled, but this approach assumes that net annual surface elevation change corresponds to the average annual accumulation layer transformed from end-of-year snow density to ice (Sold et al., 2013). Our glaciers have a low average accumulation ablation area ratio (AAR, 0.38, Table 3), and ice area ratios range from 0.38 to 0.94 (mean: 0.47). In most years, a significant amount of multi-year firn is exposed on our study glaciers, similar to other glaciers experiencing strong mass loss (Fischer, 2011; Klug et al., 2018). Firn area and column thickness losses interrupt the normal cycle of firn densification. Using the firn model of Sold et al. (2013) gives an estimated annual densification of ~0.20 m, but with high uncertainty since we lack knowledge of the required input parameters. Because of this, and because firn densification is unlikely to produce firn densities outside the range of our estimate (700 ± 100 kg m^{-3}), we

chose not to estimate firn densification in our study. Firn compaction therefore comprises one systematic uncertainty term in our analysis.

2.3 Glaciological Mass Balance

We collected glacier mass balance measurements using the glaciological method (Cogley et al., 2011) with a two-season stratigraphic approach (Østrem and Brugman, 1991). Spring glaciological field campaigns typically occurred between mid-April and mid-May, and the summer/annual balance visits took place between mid-August and mid-September (Table 2). Integration of the point measurements of B_a and B_w allows the calculation of summer balance B_s (Eqn. 1). Glacier mass balance measurements included snow depth, snow density, ablation, and kinematic GPS surveys of the glacier surface (Figure 4).

Our methods apply to the four glaciers studied by UNBC: the Zillmer, Nordic, Conrad and Kokanee glaciers. For Haig Glacier, winter mass balance measurements followed the same field protocols, but summer mass balance is derived from a combination of point observations and a distributed model of glacier melt (Marshall, 2014; Samimi and Marshall, 2017). The glacier melt model has 30 m-resolution and uses a surface energy balance, driven by AWS data collected on the upper glacier and in the glacier forefield. Illecillewaet Glacier has been monitored by Parks Canada since 2009 (Hirose and Marshall, 2013). We calculated B_{a_glac} for Illecillewaet Glacier using the contour method, as there were insufficient point measurements to apply the profile method.

Others have shown that snow depth is more variable than density (Elder et al., 1991; Pelto, 1996; Pulwicki et al., 2018), so we designed a sampling strategy that measures snow depth much more than density (an approximate sampling ratio of 25:1). We used G3 industrial aluminum probes to collect over 1,750 estimates of snow depth over the period of study. The probe can penetrate thick ice lenses and allows us to measure snow depths of up to 8 m. The boundary between snow and firn is typically made up of clearly defined ice lenses of variable thickness, which can be detected with a probe on mid-latitude glaciers (Østrem and Brugman, 1991; Pelto, 1996; Sold et al., 2013). This end-of-summer surface at our glaciers has such strength that an industrial probe can penetrate no more than a couple centimeters, in contrast with internal ice lenses in seasonal snowpack, which can be penetrated due to weak underlying support. Initially, we collected four probe measurements per location, but after two spring seasons we determined that two measurements were sufficient per location. The average σ for probe measurements for four (two) measurements was 0.14 m (0.07 m) for spring and 0.10 m (0.08 m) for late-summer. Two measurements per location allowed additional locations to be measured, since our observed low variability between proximal measurements is consistent with other studies (Beedle et al., 2014; Pelto et al., 2013).

We measured snow density with a 100 cm^3 box cutter (Hydro-Tech) in snow pits and from snow cores using a 7.25 cm-diameter Kovacs corer. Our rationale to use a snow corer was that average spring snow depth exceeded 4 m and we chose to have as many sites as possible to estimate snow density. The corer also allowed us to sample internal ice lenses, which are difficult to measure with a snow sampler (Proksch et al., 2016). We measured spring snow density at low, middle and high elevations for each glacier. If we observed an elevation trend in our density measurements, we applied a linear regression of

density and elevation to our depth measurements prior to converting these data to water equivalent (mass). When there was no linear gradient, we averaged the snow density measurements to produce a glacier-wide snow density.

We conducted nine side-by-side pit/core comparisons that revealed density measured in our snow pits was comparable, with density from snow pits about 0.2 ± 5.7% heavier than measured by subsampling snow cores (Figure S4). The mean absolute difference between pit and core density was 4.8%, similar to observations made at Alto dell'Ortles (Gabrielli et al., 2010). Methodological differences (Supplement 1) are within the range expected between duplicate field-based measurements of snow density (1-6%) and with different cutters (3-12%) (Conger and McClung, 2009; Proksch et al., 2016).

Aluminum and PVC ablation stakes were used on each glacier to measure ice and firn ablation. The stake heights were measured (±1 cm) and re-drilled during each late-summer visit. As a check on stake elevation, we measured depth to the previous snow surface for all stakes in firn, as stakes may self-drill in firn (Østrem and Brugman, 1991). Stakes were generally aligned along the centerline of a given glacier; however, we added a second transect of stakes to cover each branch to improve spatial coverage on each study site (Figure 4). Conrad Glacier also featured three latitudinal sets of ablation stakes.

To calculate mass balance, we used the profile method (Escher-Vetter et al., 2009), applied over 100-m hypsometric elevation bins. The area-altitude distribution of a given glacier was obtained using our annual late-summer ALS DEMs. The boundary of each glacier was manually delineated using the ALS DEM hillshade of the previous late-summer, and a ΔDEM (Abermann et al., 2010). We also calculated mass balance using linear regression. For Zillmer, Nordic and Conrad glaciers, we separately considered the measurements from two distinct branches or sides of each glacier and then separately applied the profile and linear methods to each branch.

To account for mass change between a given field visit and the associated ALS survey, we completed kinematic GPS surveys using a Topcon GB-1000 receiver as a rover and a second receiver as a base station. We corrected base-station data using Natural Resources Canada Precise Point Positioning (https://webapp.geod.nrcan.gc.ca/geod/tools-outils/ppp.php), before post-processed surveys using Topcon Tools. Height change observed between the ALS DEM surface and survey points were binned by elevation (Figure S5), and assigned a density based upon surface classification as determined from satellite imagery. Since ALS surveys were essentially synchronous (typically flown over two to three-days), we chose to apply the correction to the glaciological estimates of mass balance. We surveyed 2-6 control points at each site to determine the survey reliability and found that horizontal and vertical uncertainties respectively averaged ±0.04 m and ±0.06 m.

2.4 Uncertainty Assessment

We analyzed snow and ice-free terrain to derive statistical indicators of bias and data dispersion from ΔDEM over stable terrain using a late-summer DEM as a reference, and report the mean, median and normalized median absolute deviation (NMAD) over stable terrain (Table 3), which generally covered 10-20 km^2. We bias-corrected the height change over the glacier surfaces using the systematic elevation difference over stable terrain (h_{dDEM}) in the ΔDEMs. This bias correction ranged from -0.09 to 0.05 m and averaged -0.01 m. NMAD reveals random errors that are typically below ±0.3 m, with a maximum of 0.6 m

The Cryosphere Discuss., https://doi.org/10.5194/tc-2019-30
Manuscript under review for journal The Cryosphere
Discussion started: 18 February 2019

(Table 3). This maximum error occurred for Zillmer Glacier in late-summer 2017 when the separation between site visit and ALS survey was large and new snow covered the glacier during the ALS survey (Table 2).

Random uncertainty stems from three sources that we assume to be independent: i) elevation change uncertainty ($\sigma h_{\Delta DEM}$), ii) glacier zone delineation uncertainty (σA), and iii) volume to mass density conversion uncertainty ($\sigma\rho$). We define elevation change uncertainty following the methods detailed in (Menounos et al., 2018), and found an average decorrelation length of 0.75 km (Figure S3). Below, we have abbreviated our geodetic and glaciological uncertainty assessment (detailed version: Supp. 2)

For delineation of ice/firn/snow zones from satellite imagery (Figure S1), we applied a buffering method (Granshaw and Fountain, 2006) to the perimeter of each zone that was not at the glacier boundary. Our satellite imagery resolution varied from 3 to 15 m, so we chose a buffer of four times the largest pixel size, to derive an uncertainty in area per zone. This 60 m buffer accounts for uncertainty in zone delineation and changes in the positions of the zone boundaries occurring between ALS and satellite imagery acquisition dates. Total random uncertainty in volume change is:

$$\sigma\Delta V = \sqrt{(\sigma h_{\Delta DEM}(p + 5(1-p))A)^2 + (\sigma A \cdot h_{\Delta DEM})^2} \quad (3)$$

where A is the area of a given glacier and p is the percentage of surveyed area, which averaged 99.1% (Table 2). Random uncertainty on geodetic mass balance is:

$$\sigma\Delta M = \sum_i \sqrt{(\sigma\Delta V_i \cdot \rho_i)^2 + (\sigma\rho_i \cdot \Delta V)^2} \cdot \frac{A_i}{A_{tot}} \quad (4)$$

where ρ_i is individual density conversion values with associated uncertainties ($\pm\sigma\rho_i$) for spring snow, late-summer snow, firn, and ice (Table 4). Prior to being summed to produce a final uncertainty, each zone (ice/firn/snow) is considered separately for B_a, with ΔV_i and A_i the volume and area change of each zone respectively.

Firn compaction or fresh snow on the surveyed surface introduce systematic uncertainty on geodetic balance. On Drangajökull ice cap, where B_w is more than 1 m w.e. greater than our average B_w, firn compaction and fresh snow densification increased geodetic B_w by 8%. Fresh snow off-glacier was negligible in all but a few cases. We thus assume a systematic uncertainty ($\sigma\Delta M_{sys}$) of 10% on $B_{a,w}$. Collectively, random and systematic uncertainty thus yield total uncertainty in mass balance:

$$\sigma B_{geod} = \sqrt{(\sigma\Delta M)^2 + (\sigma\Delta M_{sys})^2} \quad (5)$$

To determine uncertainty in glaciological mass balance, we derive a mean density (ρ) of mass change (Table 3) and uncertainty in height change for both observations and GPS survey corrections. Uncertainty in glaciological mass balance is calculated as:

$$\sigma B_{a,w} = \sqrt{\sigma\Delta h_{glac}{}^2 \cdot \rho^2 + \sigma\rho^2 \cdot B_{a,w}{}^2} \quad (6)$$

where $\sigma\rho$ is the uncertainty on density taken to be 10% of ρ, to account for uncertainty in density measurements and extrapolation of those measurements. The uncertainty in extrapolation of glaciological observations to glacier-wide mass balance is taken as the σ of the different calculations of mass balance for each season.

For both geodetic and glaciological mass balance, B_s was derived as the difference of annual and summer balance (Eqn. 1), and thus uncertainty on B_s yields:

$$\sigma B_s = \sqrt{\sigma B_a{}^2 + \sigma B_w{}^2} \quad (7)$$

3 Results

3.1 Glaciological Versus Geodetic Balance

Comparison of seasonal balance from glaciological and geodetic methods showed strong overall agreement (Figure 5), with glaciological winter balance (B_{w_glac}) averaging 1.95 ± 0.08 m w.e., 4% greater than our geodetic estimate. Average B_{s_glac} and B_{a_glac} were 4% both more negative than B_{s_geod} and B_{a_geod} (Figure 6). Average glacier-wise difference between B_{a_glac} and B_{a_geod} was in excellent agreement (-0.03 m w.e. relative to B_{a_glac}), with an average absolute deviation of 0.10 ± 0.07 m w.e. a^{-1} between estimates (Figure 6). Glacier-wise, B_{w_glac} was 5% greater relative to B_{w_geod}, and B_{s_glac} was 4% more positive relative to B_{s_geod}. For B_w and B_s, geodetic and glaciological balance were within 20% for over 85% of cases. Average glacier-wise mean annual balance from 2015-2017 was -0.70 ± 0.15 m w.e. for both geodetic and glaciological mass balance separately (Table 3). Mean B_{s_glac} was -2.70 ± 0.13 m w.e. All glacier-wise estimates of seasonal and annual balance are within 2σ uncertainties, and only in three instances are they outside 1σ uncertainties (Figure 6).

We created a ΔDEM from the first and last late-summer DEM for each site (Figure 7) and compared calculated mass change from this ΔDEM to the sum of the individual balance years that comprised that given period (Figure 8). We found that all cumulative seasonal B_a estimates from glaciological and geodetic balance were within uncertainty (2σ) of the last-first mass change approach (Figure 8). Glaciological balance was in net more positive (average +0.09 m w.e.) and had an average absolute difference of ±0.20 m w.e. from the last-first ΔDEM. Summed B_{a_geod} agreed with our last-first estimates, with an average deviation of only 0.03 m w.e.

3.2. Glaciological density observations

Average glacier-wide snow density from snow pits and cores on a glacier-wise basis for spring is 457 ± 48 kg m^{-3}, with a coefficient of variation (CV) of 0.14 (n=74). This estimate is 13 kg m^{-3} less than our snow course-based geodetic ρ_{spring} but is within uncertainty (Table 4). For Haig Glacier, average spring density is 420 ± 45 kg m^{-3}, 20 kg m^{-3} lighter than our estimate obtained from nearby snow course measurements, but again within uncertainty. Our average late-summer glaciological density of 570 ± 20 kg m^{-3} (n=27) ranged from 536 to 617 kg m^{-3} (CV=0.04). Assigned geodetic ρ_{snow} is 18 kg m^{-3} greater than observations. Average probe depth for spring is 4.20 ± 0.06 m, with a CV of 0.33 (n=1,754). Average probe depth in late-summer is 1.85 ± 0.10 m, with a CV of 0.78 (n=777). Observed glacier-wide average snow depths are typically between 3.4 and 6.9 m, and average 4.56 ± 0.21 m. While spring snow density showed greater variability than late-summer snow density, snow depth is far more variable than snow density in both seasons.

Over the period 2015-2017 our glaciers had an average AAR of 0.38 (Table 3), with multi-year firn exposed over 13% of the glacier surface, thus leaving the remaining 49% of glacier area as bare ice. Haig Glacier is the easternmost site in our study and is in a lower-accumulation environment. It has lost nearly all its firn cover over the last 20 years, with firn area reduced to 0.06 in 2015. Excluding this site, the remaining study glaciers in the Columbia Mountains had an AAR of 0.45 with 0.15 exposed multi-year firn cover and 0.40 bare glacier ice.

3.2.1 Geodetic density sensitivity

The effect of using a regional literature-based late-summer snow density (Table 5) versus our glacier-wise glaciological density values (Table S1) depends on the amount of retained snow and glaciological density but produces a < 0.01 m w.e. decrease on average, a negligible contribution. Varying firn density by ±15% also has an average effect of ±0.01 m w.e., with the largest impact (0.04 m w.e.) experienced at Conrad Glacier in 2015, when 17% of the glacier was exposed firn. However, misclassifying a given pixel or area of glacier surface has a significant impact, as ρ_{firn} is 17% greater than snow and ρ_{ice} is 26% greater than ρ_{firn}. If we produce a single glacier-wide density (ρ) instead of distributing density based on surface classification, we change absolute magnitudes of B_{a_geod} by an average of ±0.10 m w.e. Though we did not use it for mass conversion, our ρ of B_{a_geod} ranged from 681 (Kokanee 2016) to 895 kg m^{-3} (Haig 2017) and averaged 748 ± 61 kg m^{-3}.

Applying our snow course density values for spring snow (Table 4) versus our glaciological snow density observations (Table S1) reduces average B_{w_geod} by 0.03 m w.e. (1.7%) and causes B_{w_geod} to be 5% greater than B_{w_glac} compared to 7% greater for the glaciological-density-based B_{w_geod} estimates. Glacier-wise B_{w_geod} values between the two methods differ by 1 to 13%, and only 2% on average.

3.3 Glaciological and Geodetic Balance Discrepancies

Glacier-wise estimates of seasonal and annual balance were outside 1σ uncertainties in a few cases. Conrad B_{w_glac} was 24% greater than B_{w_geod} in 2016. Snow accumulation may have occurred in the eight days between the Conrad Glacier ALS survey and field visit, as we observed over 1 m of fresh snow over four days during that interval while on Kokanee Glacier. Automatic snow weather stations near both glaciers at around 2050 m showed no accumulation, highlighting the steep balance gradient of the Columbia Mountains. Additionally, ALS acquisition failed over the terminus of the Conrad and Illecillewaet Glaciers in late-summer 2015, and our extrapolation based upon the typical gradient over the terminus may have underestimated melt (Figure 7). Kokanee Glacier B_{a_glac} in 2017 was 0.25 m w.e. more positive than B_{a_geod}, likely due to the burial of a few ablation stakes, and sub-freezing temperatures which limited our ability to take adequate snow measurements. Illecillewaet Glacier B_{w_glac} in 2017 was 46% higher than B_{w_geod}, but this difference may stem from limited B_{w_glac} observations that year (n=3). Although the terminus was not acquired in the ALS survey, we only missed 3% of glacier area.

The Cryosphere Discuss., https://doi.org/10.5194/tc-2019-30
Manuscript under review for journal The Cryosphere
Discussion started: 18 February 2019

3.4 Interannual and spatial variability

Varied climatological conditions provided a range of balance outcomes for the period of study. The lowest B_{w_glac} of the four studied winters (1.81 ± 0.12 m w.e.) occurred in 2016, yet also the least mass loss with an average B_{a_glac} of -0.36 ± 0.17 m w.e. (Figure 5). The 2016-2017 winter brought the greatest snowpack of our study period, 2.08 ± 0.18 m w.e., yet substantial mass loss was still observed (average B_{a_glac}: -0.84 ± 0.23 m w.e.). The balance year of 2014-2015 saw high sustained mass loss (average B_{a_glac} of -1.30 ± 0.13 m w.e.), despite having an B_{w_glac} within 0.01 m w.e. of 2016.

The standard deviation between the seasonal and annual balances for each glacier reveals that B_w (σ = 0.14 m w.e., 7%) experiences lower interannual variability than B_s (σ = 0.38 m w.e., 14%) and B_a (σ = 0.35 m w.e., 56%). Kokanee Glacier experienced the highest B_w in all four years 2015-2018 averaging 2.34 ± 0.30 m w.e. (Figure 6), while Haig Glacier's B_w was lowest, averaging 1.37 ± 0.11 m w.e., and the highest mass loss, averaging B_{a_glac} = -1.62 ± 0.34 m w.e.

We did not investigate the influence of crevasses for each glacier and each season, but for a test case for each glacier (n=6) we created DEMs with filled crevasses in the late-summer, and then produced a ΔDEM. We found that crevasse-free ΔDEM B_w was on average <1% smaller than our standard B_w, with discrepancies up to -0.05 m w.e or -3%. The amount of crevassing is important, however, as some of our glaciers such as the Zillmer, Nordic and Conrad feature large crevasse fields.

4 Discussion

The consistency between our geodetic and glaciological seasonal balance estimates among six glaciers over multiple years implies that high-resolution geodetic surveys can be used to reliably measure both winter and summer mass balance. Our study builds upon previous work that established the feasibility of geodetic methods to accurately produce B_w (Belart et al., 2017; Sold et al., 2013), and B_a (Klug et al., 2018). While others show that geodetic surveys can be applied for a single winter (Belart et al., 2017; Sold et al., 2013) or for one glacier over a number of years (Klug et al., 2018), our study demonstrates remotely-measured seasonal balance is possible for widely varying rates of accumulation and ablation for multiple glaciers across entire mountain ranges.

4.1 Geodetic seasonal Balance

Our small estimate of σh_{dDEM} and bias correction (Table 3) highlight that height change uncertainty is generally minor; these terms are still important to quantify, however (Joerg et al., 2012; Klug et al., 2018). As described below, density distribution and conversion factors comprise a large portion of total mass change uncertainty, with firn compaction, fresh snow at the time of ALS acquisition, and crevasses also contributing.

The spatial coverage of ALS is far superior to glaciological observations; however, isolating the snow-depth portion of surface height change at a given location is difficult and requires detailed input data (Belart et al., 2017; Sold et al., 2013). While we can develop balance gradients from glaciological data, we have not attempted to do so using our ALS data. To date, studies have differenced their glaciological and geodetic data regarding surface height change and assigned the difference as a

combination of vertical ice velocity and firn compaction (Beedle et al., 2014; Belart et al., 2017; Sold et al., 2013) or used full-Stokes ice flow model with a bedrock DEM, a surface DEM, and GPS-observed horizontal velocities as inputs (Belart et al., 2017). Then, after applying a simple firn model, vertical ice velocity is estimated. While this method appears robust, and differencing of our glaciological observations of height change from our ΔDEMs produces realistic emergence/submergence velocities, it is beyond the scope of this study.

4.1.1 Density distribution and conversion factors

Converting volume to mass change is a major challenge for geodetic studies (Huss, 2013; Moholdt et al., 2010). Over multiple years to decades, a constant value of density can produce tolerable uncertainty of mass change (Huss, 2013). For shorter timescales, and particularly for seasonal balance, a careful consideration of density is necessary (Klug et al., 2018). Klug et al (2018) used ALS intensity data and satellite imagery for a pixel-based classification of the glacier surface as firn and ice. Our mapping built on this work and mapped areas of ice, but also distinguished between snow and firn. To investigate the influence of density assumptions, we compare using independent estimates of density and our glaciological data to inform our geodetic estimates, to better constrain the uncertainty on, and compare against, glaciological seasonal balance. Varying the density assigned to each surface class to the maximum and minimum values within our conservative uncertainties has minor effect on seasonal balance but failing to distribute them appropriately has a large impact. If a single density value is used, the range of values of ρ of B_{a_geod} indicates that a value close to 750 ± 60 kg m^{-3} would be most appropriate for seasonal mass change over this period (Table 3). Given the spread ρ between glaciers, however, a glacier-wise ρ would be best.

Like Klug et al. (2018), our applied firn density was selected based on a core from a temperate glacier in the Alps (Ambach et al., 1966), and our in-situ density measurements for firn ≥2 years old matched this value (Table 4). Our glaciological density values for one-year-old firn and late-summer snow density are respectively 13.1 and 22.4% (Table 4) less than the assumed value of 700 kg m^{-3} for both snow and firn taken by Klug et al. (2018). Had we also taken this value for our snow-covered areas, we would have introduced a negative bias to B_{a_geod}. As glacier mass loss rates continue to accelerate (Menounos et al., 2018), it is reasonable to expect more and older exposed firn during the ablation season, which for geodetic studies, may imply a higher density conversion factor for firn.

Applying glaciological late-summer snow density versus our independent regional average density (Table 5) had little effect on B_{a_geod}. Future geodetic studies should use the best available local data, however, as different regions and mountain ranges have different late-summer densities (Table 5).

Using our glaciological winter density values to produce B_{w_geod} estimates resulted in a slightly greater discrepancy relative to B_{w_glac} than applying our snow-course-based densities (Table 3). The two B_{w_geod} estimates produced similar results in net, however, with glacier-wise only a 2% difference between B_{w_geod} estimates. Our regression-slope approach (Figure 3) to adjust glaciological observations of spring snow density (Table S1), is suitable over the period mid-April through late-May, but we caution against its use for other periods of the year when densification is far slower and less predictable. For Haig Glacier, a linear relation also appears to exist between mid-April through late-May (Marshall, 2012, p.18, Fig. 2.3). Coincident with our

spring field visits and ALS surveys, springtime warming is influencing the snowpack, and homogenizing snow density (Adams, 1976; Elder et al., 1991). In western Canada, onset of snow melt is occurring earlier on average relative to 1970-2006 (Déry et al., 2009). However, great variability still exists, with the first significant warming event of the spring occurring in the Columbia and Rocky Mountains between early April and early May (Marshall, 2012). The tendency for a more homogenous snow density, and lack of altitudinal trend both lend credence to using a single snow density (Fausto et al., 2018; McGrath et al., 2018).

4.1.2 Firn compaction

While firn compaction is only incorporated in our uncertainty analysis, others estimate its effect to derive B_{w_geod} (Belart et al., 2017; Sold et al., 2013), but not for B_{a_geod} (Klug et al., 2018). For B_{w_geod}, firn compaction was estimated based upon the annual balance in the accumulation zone over a decade (Sold et al., 2013) or over a single balance year (Belart et al., 2017). The accumulation areas on our glaciers are in constant flux, however, and are nearly always discontinuous. Exposed firn is the norm, implying that the firn zone on our study sites is shrinking in area and thickness, interrupting the cycle of firnification, and invalidating firnification models which assume that one annual layer is transformed from snow to ice annually. Nevertheless, a carefully considered treatment of firn could improve seasonal geodetic balance estimates, but as demonstrated by Belart et al. (2017), firn and fresh snow densification have little effect on B_{w_geod} if the magnitude of winter accumulation is large. For regions with low winter balance, compaction would have a larger relative influence on B_w. We also chose not to apply a firn correction since it requires glaciological measurements that we purposely withheld in order to evaluate the feasibility of measuring seasonal balance without surface observations from the glaciers.

4.1.3 Fresh Snow

Presence of fresh snow at the time of acquisition is a challenge for any geodetic survey estimating mass change (Belart et al., 2017; Joerg et al., 2012; Klug et al., 2018). Fresh snow can change the height of the target surface by tens of centimeters. Our bias-correction of ΔDEM height change (Figure S2, Table 3) corrected for small quantities of fresh snow, assuming that snow was present over stable terrain. In late-summer, we could detect fresh snow visually, as a hillshade of the glacier surface at 1-m resolution captures intricate details which are easily disguised by snow depths of 0.2 m or more. Off-glacier, the depth and distribution of fresh snow is variable due to the thermal properties of bedrock and other surfaces, and redistribution. In spring, we are unable to detect fresh snow as the only snow-free pixels in our scenes are typically rock faces with extreme slopes and tree-tops. Our $\sigma\Delta M_{sys}$ attempts to approximate the systematic uncertainty introduced by fresh snow and firn compaction.

4.1.4 Crevasses and internal mass change

Crevasses can affect both B_{w_geod}, and B_{w_glac} since crevasses bridged by winter snowpack will overestimate B_{w_geod} snow volume, and crevasses filled by snow would not be captured by B_{w_glac}. We produced 'crevasse-free' glacier surfaces by

resampling late-summer DEMs to 10 m using the maximum elevations within the smoothing window to avoid in-crevasse height measurements. Using the 10 m 'crevasse-free' DEMs versus the original 1-m DEMs had little influence on B_{w_geod}, with only the Zillmer and Nordic glaciers showing a difference >1%. We did not extend these test cases to cover B_{a_geod} estimates because the number and area of exposed crevasses varied little year to year. On Hintereisferner, crevasse effects biased B_{a_geod} by only 0.03% (-0.047 m w.e.) over a decade (Klug et al., 2018). Despite the small influence of crevassing on B_{a_geod} observed in this study, additional studies should quantify the magnitude of this bias. Our field operations have been impacted by the melting out of crevasses: as strongly negative years are becoming the norm, and glacier flux is likely decreasing, crevasses are exposed for longer periods of time, and slower to close. This means that the total void area of crevasses is increasing due to ablation, which we have observed on Conrad, Zillmer, Nordic, and Haig glaciers, which could possibly increase their influence on B_w.

Geodetic balance implicitly includes internal and basal mass change, which are not captured by the glaciological method. Studies of these processes are rare and are based upon estimates rather than verified measurements. Estimates of annual mass loss from geothermal heat, potential energy released by runoff or ice motion, and basal friction are typically around 0.01 to 0.10 m w.e. (Huss et al., 2009; Oerlemans, 2013; Sold et al., 2016). Crevasses and internal processes likely combine to be 0 to 4% of the magnitude of average annual ablation per literature estimates (e.g. Klug et al., 2018; Sold et al., 2016), and thus do not appear to be important contributors to seasonal balance in the Columbia Mountains. Further, the capacity for the firn reservoir of a glacier to retain meltwater may be approximated by a simple firn model, and would tend to increase mass balance, possibly offsetting typical basal/internal mass loss, but would not be captured by geodetic or glaciological measurements.

4.2 Glaciological seasonal balance

Observational biases include the representativeness of sampling sites and number of measurements (Cogley, 1999; Fountain and Vecchia, 1999), and the extrapolation of those measurements to produce a glacier-wide balance estimate (Sold et al., 2016; Thibert and Vincent, 2009).The difficulty of comparability between methods and sites (Cogley, 1999; Fountain and Vecchia, 1999) is an ongoing challenge due to logistical and financial obstacles to in-situ mass balance studies. Areas of a glacier may be inaccessible, and preferred paths chosen for measurement may be biased to areas which better retain snowpack for safety purposes (Østrem and Brugman, 1991). Our glaciological measurement densities ranged from 0.5 to 18.5 points km^{-2} (Table 2), whereas our ALS data had around one million points km^{-2}.

4.2.1 Snow depth

We observed best agreement between geodetic and glaciological measurements of winter balance during years of dense field surveys. Safety or logistical constraints prevented us from completing all transects of snow depth measurements in some years, and again, greater discrepancy was found in cases where our coverage was incomplete. In both spring and late-summer, we encountered internal ice layers at some or all sites. Ice lenses were most common in the accumulation zone, but they were also found in the ablation zone in spring. These internal layers form via rain-on-snow events (McCabe et al., 2007) or, as the year

progresses, via internal storage of meltwater (Pfeffer and Humphrey, 1996). Ice layers 2-6 cm thick were present nearly every year in the accumulation zone of the Conrad Glacier. We were able to penetrate these layers and successfully measure spring snow depth using our industrial avalanche probe. A conventional avalanche probe is unsuitable for glaciological observations in our region.

The greater B_{w_geod} of 2016 on Conrad Glacier may in part due to the late-summer 2015 ALS survey missing the lowest reaches of the glacier, preventing calculation of surface height change for that portion of the glacier. We estimated the snow depth for the lower reaches of the glacier based upon the ratio of snow depth observed there for other years relative to the rest of glacier, and snow depths along the cut-off margin. The B_w discrepancy for Zillmer Glacier in 2016 is likely due to glaciological sampling bias, as the east transect (Figure 4), which has a lesser snowpack, was not sampled, and the 30-day difference between field and ALS survey date (Table 2) may not be fully resolved by the GPS survey correction.

4.2.2 Mass change between measurements

Previous studies account for mass change that occurs between measurements by using a distributed temperature index model (Sold et al., 2013) or degree-day model (Belart et al., 2017), but these models do not account for snow gain. We utilized in-situ GPS surveys of the glacier height which were then compared with ALS DEMs. We binned and averaged our height change estimates by 100 m elevation bands (Figure S5), and then applied a density to each band based on satellite observations of a given surface class. Limitations in our approach include: 1) fresh snowfall in spring or late-summer, between the GPS and ALS surveys; and 2) significant densification of the snowpack in spring. A weather station situated proximal to the glacier that could be used to drive a surface mass balance model (Fitzpatrick et al., 2017) would be required to capture local changes in glacier mass due to precipitation events and compaction. Terrain presents a further challenge to kinematic GPS survey observations. The GPS antenna is securely mounted in the backpack of a field member, but the measured height of the antenna above the glacier surface may vary due to the uneven glacier terrain, particularly during travel on steep slopes (Beedle et al., 2014).

Our median dates of late-summer glaciological visits and geodetic surveys are September 6th, and September 18th respectively (Table 2). Snowfall can occur at any time of the year in the Columbia and Rocky Mountains (Schnorbus et al., 2014), and in late August, throughout September, and even into early October, either melt or accumulation can prevail (Marshall, 2014). Lowering of the surface via ablation post ALS survey dates (Table 2) is not accounted for and would cause an underestimated winter snowpack. While our methods are comparable year-to-year, and between sites, our B_w and B_s values are not the total amount of snow and runoff during a year. We do not include snow which falls between May and August and melts off and cannot measure ablation occurring after our ALS survey or glaciological visit, whichever occurs later. Thus, our B_w and B_s values represent a low threshold estimate of runoff contributions from snow and ice melt.

The close agreement between geodetic and glaciological seasonal balance estimates might be fortuitous in that most of our glaciers have moderate mass turnover; regions with low mass turnover would require treatment of more ancillary factors such as firn compaction.

The Cryosphere Discuss., https://doi.org/10.5194/tc-2019-30
Manuscript under review for journal The Cryosphere
Discussion started: 18 February 2019

5. Conclusions

Estimates of seasonal mass balance presented here show strong agreement between glaciological and geodetic methods on a glacier-by-glacier basis, and are within 1σ uncertainties for average winter, summer, and annual balance. These independent estimates of seasonal mass change accord over three years from glaciers separated by hundreds of kilometers. Our findings suggest that high-resolution geodetic methods, such as from ALS (Klug et al., 2018; Sold et al., 2013), aerial photogrammetry (Nolan et al., 2015), and stereo satellite imagery (Belart et al., 2017; Berthier et al., 2014) can be used to produce accurate seasonal and annual balance estimates over large areas. The quality of geodetic annual balance estimates depends more on distributing density via surface classification (Klug et al., 2018), than on the density values themselves. The spatial coverage, density of observations, and measurement precision of high-resolution geodetic terrain analysis compensates for errors associated with fresh snow and firn compaction, internal and basal mass change, and crevasses (Belart et al., 2017; Klug et al., 2018). The minimal impact of these factors on mass balance stems from the large mass changes observed at our sites, as reported elsewhere (Belart et al., 2017; Klug et al., 2018). For glaciers with low mass turnover, errors introduced by firn compaction, crevasses, and fresh snow may be considerable larger than observed in our study.

Our estimate of spring snow density for geodetic measurements based upon provincial snow course observations (Figure 2) is within the uncertainty of our measured glaciological spring snow density (Table 4). Estimates of end-of-season snow density introduce a possible bias, but given the regional consistency of late-summer snow density, and the overall lack of a density-altitude gradient in spring, using a single snow density is a robust method for converting snow depth to water equivalence (Fausto et al., 2018; McGrath et al., 2018).

The hydrologic cycle of western North America is dominated by snowfall in the mountains, but observations of alpine snowpack above 2000 m asl are sparse. As climate continues to change, there is a growing need for a more detailed understanding of the seasonal balance of glaciers and snowpack. Geodetic methods are needed to supplement in-situ observations across many mountain regions in order to address the contribution of glacier to sea level rise and changes in freshwater availability. To date, the majority of high-resolution geodetic balance studies of seasonal or annual balance have been conducted in the European Alps, where extensive, multi-decadal glaciological data are available (Klug et al., 2018; Sold et al., 2013, 2016). Our study suggests that geodetic methods can be used to assess seasonal balance of glaciers, even in mountain ranges lacking long-term records of mass balance, as long as density is carefully considered (Belart et al., 2017; Klug et al., 2018). Recent advances in satellite technology (Berthier et al., 2014; Marti et al., 2016) suggest that such efforts can be made with increasing spatial and temporal coverage, greatly adding to our understanding of mountain hydrology, on which so much depends, but so little is known.

Acknowledgements

We acknowledge financial support from the Columbia Basin Trust, BC Hydro, the Pacific Institute for Climate Solutions, the Natural Resources and Engineering Research Council of Canada, and the Canada Chairs Program. Ben Pelto conducted the

field work with the help of many invaluable volunteers, and conducted the bulk of the ALS processing, and analysis. Analysis of Haig Glacier was conducted by Shawn Marshall. The authors wish to thank All authors contributed to the writing of the manuscript. The authors declare that they have no conflict of interest.

References

Abermann, J., Fischer, A., Lambrecht, A. and Geist, T.: On the potential of very high-resolution repeat DEMs in glacial and periglacial environments, The Cryosphere, 4(1), 53, 2010.

Adams, W.: Areal differentiation of snow cover in east central Ontario, Water Resour. Res., 12(6), 1226–1234, 1976.

Ambach, W., Bortenschlager, S. and Eisner, H.: Pollen-analysis investigation of a 20 m. Firn Pit on the Kesselwandferner (Ötztal Alps), J. Glaciol., 6(44), 233–236, 1966.

Bahr, D. B., Dyurgerov, M. and Meier, M. F.: Sea-level rise from glaciers and ice caps: A lower bound, Geophys. Res. Lett., 36(3), doi:10.1029/2008GL036309, 2009.

Barnett, T. P., Adam, J. C. and Lettenmaier, D. P.: Potential impacts of a warming climate on water availability in snow-dominated regions, Nature, 438(7066), 303–309, doi:10.1038/nature04141, 2005.

Beedle, M. J., Menounos, B. and Wheate, R.: An evaluation of mass-balance methods applied to Castle Creek Glacier, British Columbia, Canada, J. Glaciol., 60(220), 262–276, doi:10.3189/2014JoG13J091, 2014.

Belart, J. M. C., Berthier, E., Magnússon, E., Anderson, L. S., Pálsson, F., Thorsteinsson, T., Howat, I. M., Aðalgeirsdóttir, G., Jóhannesson, T. and Jarosch, A. H.: Winter mass balance of Drangajökull ice cap (NW Iceland) derived from satellite sub-meter stereo images, The Cryosphere, 11(3), 1501–1517, doi:10.5194/tc-11-1501-2017, 2017.

Benson, C. S.: Stratigraphic studies in the snow and firn of the Greenland ice sheet, Cold Regions Research and Engineering Lab Hanover NH., 1962.

Berthier, E., Vincent, C., Magnússon, E., Gunnlaugsson, Á., Pitte, P., Le Meur, E., Masiokas, M., Ruiz, L., Pálsson, F. and Belart, J.: Glacier topography and elevation changes derived from Pléiades sub-meter stereo images, Cryosphere, 8(6), 2275–2291, 2014.

Bevington, A., Gleason, H., Giroux-Bougard, X. and de Jong, J. T.: A Review of Free Optical Satellite Imagery for Watershed-Scale Landscape Analysis, Conflu. J. Watershed Sci. Manag., 2(2), 2018.

Bolch, T., Menounos, B. and Wheate, R.: Landsat-based inventory of glaciers in western Canada, 1985–2005, Remote Sens. Environ., 114(1), 127–137, doi:10.1016/j.rse.2009.08.015, 2010.

Bollmann, E., Sailer, R., Briese, C., Stötter, J. and Fritzmann, P.: Potential of airborne laser scanning for geomorphologic feature and process detection and quantifications in high alpine mountains, Z. Für Geomorphol. Suppl. Issues, 55(2), 83–104, 2011.

Brahney, J., Weber, F., Foord, V., Janmaat, J. and Curtis, P. J.: Evidence for a climate-driven hydrologic regime shift in the Canadian Columbia Basin, Can. Water Resour. JournalRevue Can. Ressour. Hydr., 42(2), 179–192, 2017.

Bretherton, C. S., Widmann, M., Dymnikov, V. P., Wallace, J. M. and Bladé, I.: The effective number of spatial degrees of freedom of a time-varying field, J. Clim., 12(7), 1990–2009, 1999.

Clarke, G. K. C., Anslow, F. S., Jarosch, A. H., Radić, V., Menounos, B., Bolch, T. and Berthier, E.: Ice Volume and Subglacial Topography for Western Canadian Glaciers from Mass Balance Fields, Thinning Rates, and a Bed Stress Model, J. Clim., 26(12), 4282–4303, doi:10.1175/JCLI-D-12-00513.1, 2013.

Clarke, G. K. C., Jarosch, A. H., Anslow, F. S., Radić, V. and Menounos, B.: Projected deglaciation of western Canada in the twenty-first century, Nat. Geosci., doi:10.1038/ngeo2407, 2015.

Cogley, J., Hock, R., Rasmussen, L., Arendt, A., Bauder, A., Braithwaite, R., Jansson, P., Kaser, G., Möller, M. and Nicholson, L.: Glossary of glacier mass balance and related terms, IHP-VII technical documents in hydrology No. 86, IACS Contribution No. 2, Int. Hydrol. Program UNESCO Paris, 2011.

Cogley, J. G.: Effective sample size for glacier mass balance, Geogr. Ann. Ser. Phys. Geogr., 81(4), 497–507, 1999.

Cohen, S. J., Miller, K. A., Hamlet, A. F. and Avis, W.: Climate change and resource management in the Columbia River Basin, Water Int., 25(2), 253–272, 2000.

Conger, S. M. and McClung, D. M.: Comparison of density cutters for snow profile observations, J. Glaciol., 55(189), 163–169, 2009.

Cuffey, K. M. and Paterson, W. S. B.: The physics of glaciers, Academic Press., 2010.

Dadic, R., Mott, R., Lehning, M. and Burlando, P.: Wind influence on snow depth distribution and accumulation over glaciers, J. Geophys. Res., 115(F1), doi:10.1029/2009JF001261, 2010.

Demarchi, D. A.: An introduction to the ecoregions of British Columbia., 2011.

Déry, S. J., Stahl, K., Moore, R. D., Whitfield, P. H., Menounos, B. and Burford, J. E.: Detection of runoff timing changes in pluvial, nival, and glacial rivers of western Canada, Water Resour. Res., 45(4), doi:10.1029/2008WR006975, 2009.

Elder, K., Dozier, J. and Michaelsen, J.: Snow accumulation and distribution in an alpine watershed, Water Resour. Res., 27(7), 1541–1552, 1991.

Escher-Vetter, H., Kuhn, M. and Weber, M.: Four decades of winter mass balance of Vernagtferner and Hintereisferner, Austria: methodology and results, Ann. Glaciol., 50(50), 87–95, doi:10.3189/172756409787769672, 2009.

Fausto, R. S., Box, J. E., Vandecrux, B., van As, D., Steffen, K., MacFerrin, M. J., Machguth, H., Colgan, W., Koenig, L. S., McGrath, D., Charalampidis, C. and Braithwaite, R. J.: A Snow Density Dataset for Improving Surface Boundary Conditions in Greenland Ice Sheet Firn Modeling, Front. Earth Sci., 6, 51, doi:10.3389/feart.2018.00051, 2018.

Fischer, A.: Comparison of direct and geodetic mass balances on a multi-annual time scale, The Cryosphere, 5(1), 107–124, doi:10.5194/tc-5-107-2011, 2011.

Fitzpatrick, N., Radić, V. and Menounos, B.: Surface Energy Balance Closure and Turbulent Flux Parameterization on a Mid-Latitude Mountain Glacier, Purcell Mountains, Canada, Front. Earth Sci., 5, 67, 2017.

Fountain, A. G. and Vecchia, A.: How many stakes are required to measure the mass balance of a glacier?, Geogr. Ann. Ser. Phys. Geogr., 81(4), 563–573, 1999.

Gabrielli, P., Carturan, L., Gabrieli, J., Dinale, R., Krainer, K., Hausmann, H., Davis, M., Zagorodnov, V., Seppi, R., Barbante, C., Dalla Fontana, G. and Thompson, L. G.: Atmospheric warming threatens the untapped glacial archive of Ortles mountain, South Tyrol, J. Glaciol., 56(199), 843–853, doi:10.3189/002214310794457263, 2010.

Granshaw, F. D. and Fountain, A. G.: Glacier change (1958–1998) in the north Cascades national park complex, Washington, USA, J. Glaciol., 52(177), 251–256, 2006.

Hägeli, P. and McClung, D. M.: Avalanche characteristics of a transitional snow climate—Columbia Mountains, British Columbia, Canada, Cold Reg. Sci. Technol., 37(3), 255–276, 2003.

Hamlet, A. F. and Lettenmaier, D. P.: Columbia River streamflow forecasting based on ENSO and PDO climate signals, J. Water Resour. Plan. Manag., 125(6), 333–341, 1999.

Hamlet, A. F., Mote, P. W., Clark, M. P. and Lettenmaier, D. P.: Effects of temperature and precipitation variability on snowpack trends in the Western United States*, J. Clim., 18(21), 4545–4561, 2005.

Helfricht, K., Kuhn, M., Keuschnig, M. and Heilig, A.: Lidar snow cover studies on glaciers in the Ötztal Alps (Austria): comparison with snow depths calculated from GPR measurements, The Cryosphere, 8(1), 41–57, doi:10.5194/tc-8-41-2014, 2014.

Herron, M. M. and Langway, C. C.: Firn densification: an empirical model, J. Glaciol., 25(93), 373–385, 1980.

Hirose, J. M. R. and Marshall, S. J.: Glacier Meltwater Contributions and Glaciometeorological Regime of the Illecillewaet River Basin, British Columbia, Canada, Atmosphere-Ocean, 51(4), 416–435, doi:10.1080/07055900.2013.791614, 2013.

Huss, M.: Density assumptions for converting geodetic glacier volume change to mass change, The Cryosphere, 7(3), 877–887, doi:10.5194/tc-7-877-2013, 2013.

Huss, M. and Hock, R.: A new model for global glacier change and sea-level rise, Front. Earth Sci., 3, doi:10.3389/feart.2015.00054, 2015.

Huss, M., Bauder, A. and Funk, M.: Homogenization of long-term mass-balance time series, Ann. Glaciol., 50(50), 198–206, 2009.

Joerg, P. C., Morsdorf, F. and Zemp, M.: Uncertainty assessment of multi-temporal airborne laser scanning data: A case study on an Alpine glacier, Remote Sens. Environ., 127, 118–129, doi:10.1016/j.rse.2012.08.012, 2012.

Jost, G., Moore, R. D., Menounos, B. and Wheate, R.: Quantifying the contribution of glacier runoff to streamflow in the upper Columbia River Basin, Canada, Hydrol. Earth Syst. Sci., 16(3), 849–860, doi:10.5194/hess-16-849-2012, 2012.

Kääb, A.: Remote sensing of mountain glaciers and permafrost creep, Geographisches Institut der Universität Zürich, Zürich., 2005.

Klug, C., Bollmann, E., Galos, S. P., Nicholson, L., Prinz, R., Rieg, L., Sailer, R., Stötter, J. and Kaser, G.: Geodetic reanalysis of annual glaciological mass balances (2001–2011) of Hintereisferner, Austria, The Cryosphere, 12(3), 833–849, doi:10.5194/tc-12-833-2018, 2018.

Machguth, H., Eisen, O., Paul, F. and Hoelzle, M.: Strong spatial variability of snow accumulation observed with helicopter-borne GPR on two adjacent Alpine glaciers, Geophys. Res. Lett., 33(13), doi:10.1029/2006GL026576, 2006.

Marshall, S.: The Cryosphere, Princeton University Press, Princeton., 2012.

Marshall, S. J.: Meltwater run-off from Haig Glacier, Canadian Rocky Mountains, 2002-2013, Hydrol. Earth Syst. Sci., 18(12), 5181, 2014.

Marti, R., Gascoin, S., Berthier, E., Pinel, M. de, Houet, T. and Laffly, D.: Mapping snow depth in open alpine terrain from stereo satellite imagery, The Cryosphere, 10(4), 1361–1380, 2016.

McCabe, G. J., Hay, L. E. and Clark, M. P.: Rain-on-Snow Events in the Western United States, Bull. Am. Meteorol. Soc., 88(3), 319–328, doi:10.1175/BAMS-88-3-319, 2007.

McGrath, D., Sass, L., O'Neel, S., Arendt, A., Wolken, G., Gusmeroli, A., Kienholz, C. and McNeil, C.: End-of-winter snow depth variability on glaciers in Alaska, J. Geophys. Res. Earth Surf., 120(8), 1530–1550, doi:10.1002/2015JF003539, 2015.

McGrath, D., Sass, L., O'Neel, S., McNeil, C., Candela, S. G., Baker, E. H. and Marshall, H.-P.: Interannual snow accumulation variability on glaciers derived from repeat, spatially extensive ground-penetrating radar surveys, The Cryosphere, 12(11), 3617–3633, doi:10.5194/tc-12-3617-2018, 2018.

Menounos, B., Hugonnet, R., Shean, D., Gardner, A., Howat, I., Berthier, E., Pelto, B., Tennant, C., Shea, J. and Noh, M.: Heterogeneous changes in western North American glaciers linked to decadal variability in zonal wind strength, Geophys. Res. Lett., 2018.

Miller, M. M. and Pelto, M. S.: Mass balance measurements on the Lemon Creek Glacier, Juneau Icefield, Alaska 1953–1998, Geogr. Ann. Ser. Phys. Geogr., 81(4), 671–681, 1999.

Moholdt, G., Nuth, C., Hagen, J. O. and Kohler, J.: Recent elevation changes of Svalbard glaciers derived from ICESat laser altimetry, Remote Sens. Environ., 114(11), 2756–2767, doi:10.1016/j.rse.2010.06.008, 2010.

Najafi, M. R., Zwiers, F. and Gillett, N.: Attribution of the Observed Spring Snowpack Decline in British Columbia to Anthropogenic Climate Change, J. Clim., 30(11), 4113–4130, doi:10.1175/JCLI-D-16-0189.1, 2017.

Nolan, M., Larsen, C. and Sturm, M.: Mapping snow depth from manned aircraft on landscape scales at centimeter resolution using structure-from-motion photogrammetry, The Cryosphere, 9(4), 1445–1463, doi:10.5194/tc-9-1445-2015, 2015.

Oerlemans, J.: A note on the water budget of temperate glaciers, The Cryosphere, 7(5), 1557–1564, 2013.

Oerlemans, J., Anderson, B., Hubbard, A., Huybrechts, P., Johannesson, T., Knap, W. H., Schmeits, M., Stroeven, A. P., Van de Wal, R. S. W., Wallinga, J. and others: Modelling the response of glaciers to climate warming, Clim. Dyn., 14(4), 267–274, 1998.

Ohmura, A.: Observed mass balance of mountain glaciers and Greenland ice sheet in the 20th century and the present trends, Surv. Geophys., 32(4–5), 537–554, 2011.

Østrem, G. and Brugman, M.: Mass balance measurement techniques, Man. Field Off. Work Natl. Hy-Drology Res. Inst. NHRI Sci. Rep., (4), 1991.

Pelto, M. S.: Annual net balance of North Cascade glaciers, 1984-94, J. Glaciol., 42(140), 3–9, 1996.

Pelto, M. S.: The current disequilibrium of North Cascade glaciers, Hydrol. Process., 20(4), 769–779, doi:10.1002/hyp.6132, 2006.

Pelto, M. S. and Miller, M. M.: Mass balance of the Taku Glacier, Alaska from 1946 to 1986, Northwest Sci., 64(3), 1990.

Pelto, M. S. and Riedel, J.: Spatial and temporal variations in annual balance of North Cascade glaciers, Washington 1984-2000, Hydrol. Process., 15(18), 3461–3472, doi:10.1002/hyp.1042, 2001.

Pelto, M. S., Kavanaugh, J. and McNeil, C.: Juneau icefield mass balance program 1946–2011, Earth Syst. Sci. Data, 5(2), 319–330, 2013.

Pfeffer, W. and Humphrey, N.: Determination of timing and location of water movement and ice-layer formation by temperature measurements in sub-freezing snow, J. Glaciol., 42(141), 292–304, 1996.

Proksch, M., Rutter, N., Fierz, C. and Schneebeli, M.: Intercomparison of snow density measurements: bias, precision, and vertical resolution, The Cryosphere, 10(1), 371–384, 2016.

Pulwicki, A., Flowers, G. E., Radić, V. and Bingham, D.: Estimating winter balance and its uncertainty from direct measurements of snow depth and density on alpine glaciers, J. Glaciol., 1–15, doi:10.1017/jog.2018.68, 2018.

Radić, V. and Hock, R.: Regionally differentiated contribution of mountain glaciers and ice caps to future sea-level rise, Nat. Geosci., 4(2), 91–94, doi:10.1038/ngeo1052, 2011.

Ragettli, S., Immerzeel, W. W. and Pellicciotti, F.: Contrasting climate change impact on river flows from high-altitude catchments in the Himalayan and Andes Mountains, Proc. Natl. Acad. Sci., 113(33), 9222–9227, 2016.

Samimi, S. and Marshall, S. J.: Diurnal Cycles of Meltwater Percolation, Refreezing, and Drainage in the Supraglacial Snowpack of Haig Glacier, Canadian Rocky Mountains, Front. Earth Sci., 5, 6, 2017.

Schnorbus, M., Werner, A. and Bennett, K.: Impacts of climate change in three hydrologic regimes in British Columbia, Canada, Hydrol. Process., 28(3), 1170–1189, doi:10.1002/hyp.9661, 2014.

Sinclair, K. and Marshall, S.: Temperature and vapour-trajectory controls on the stable-isotope signal in Canadian Rocky Mountain snowpacks, J. Glaciol., 55(191), 485–498, 2009.

Sold, L., Huss, M., Hoelzle, M., Andereggen, H., Joerg, P. C. and Zemp, M.: Methodological approaches to infer end-of-winter snow distribution on alpine glaciers, J. Glaciol., 59(218), 1047–1059, doi:10.3189/2013JoG13J015, 2013.

Sold, L., Huss, M., Eichler, A., Schwikowski, M. and Hoelzle, M.: Recent accumulation rates of an alpine glacier derived from firn cores and repeated helicopter-borne GPR, Cryosphere Discuss., 8(4), 4431–4462, doi:10.5194/tcd-8-4431-2014, 2014.

Sold, L., Huss, M., Machguth, H., Joerg, P. C., Leysinger Vieli, G., Linsbauer, A., Salzmann, N., Zemp, M. and Hoelzle, M.: Mass balance re-analysis of Findelengletscher, Switzerland; benefits of extensive snow accumulation measurements, Front. Earth Sci., 4, 18, 2016.

Stahl, K. and Moore, R. D.: Influence of watershed glacier coverage on summer streamflow in British Columbia, Canada, Water Resour. Res., 42(6), doi:10.1029/2006WR005022, 2006.

Thibert, E. and Vincent, C.: Best possible estimation of mass balance combining glaciological and geodetic methods, Ann. Glaciol., 50(50), 112–118, 2009.

WGMS: Fluctuations of Glaciers Database, 2017.

The Cryosphere Discuss., https://doi.org/10.5194/tc-2019-30
Manuscript under review for journal The Cryosphere
Discussion started: 18 February 2019

Table 1: Glacier specific details. Firn ratio is area of glacier covered by multi-year firn: exposed firn and accumulation area from 2015 imagery.

Glacier	Area (km^2)	Max Elev. (m)	Min Elev. (m)	Range (m)	Mean Elev. (m)	Length (km)	Firn Ratio	Aspect
Zillmer	5.43	2860	1860	1000	2380	5.59	0.59	NW
Nordic	3.39	2990	2065	925	2515	3.30	0.62	N
Illecillewaet	7.72	2908	2147	761	2532	4.29	0.48	WNW
Haig	2.62	2870	2461	409	2660	2.45	0.06	SE
Conrad	11.45	3235	1825	1410	2595	12.18	0.58	N
Kokanee	1.79	2805	2220	585	2585	2.20	0.48	N

670

Table 2: Acquisition date and number of observation locations (n) for glaciological visits and geodetic survey dates. Field dates are median date of glacier visit.

Year	Glacier	Late-summer Glac.	n	Late-summer Geod.	Cover (%)	Winter Glac.	n	Winter Geod.	Cover (%)
2015	Zillmer	8/23/2015	23	10/3/2015	100	5/30/2015	20	4/19/2015	100
2016	Zillmer	8/15/2016	23	9/14/2016	100	4/14/2016	46	4/18/2016	100
2017	Zillmer	8/22/2017	26	11/3/2017	100	4/13/2017	31	5/20/2017	100
2018	Zillmer	na	na	na	na	5/19/2018	42	4/29/2018	100
2014	Nordic	8/29/2014	8	9/11/2014	100	4/27/2014	16	na	na
2015	Nordic	8/31/2015	10	9/11/2015	99	5/1/2015	20	4/19/2015	100
2016	Nordic	8/21/2016	21	9/12/2016	99	5/2/2016	28	4/17/2016	100
2017	Nordic	9/14/2017	18	9/27/2017	100	5/1/2017	21	5/21/2017	100
2018	Nordic	na	na	na	na	5/1/2018	21	4/26/2018	100
2015	Illecillewaet	9/24/2015	9	9/11/2015	97	na	na	4/19/2015	100
2016	Illecillewaet	9/13/2016	7	9/12/2016	100	na	na	4/17/2016	100
2017	Illecillewaet	9/27/2017	7	9/17/2017	100	5/19/2017	3	5/21/2017	100
2018	Illecillewaet	na	na	na	na	na	na	4/26/2018	100
2015	Haig	9/12/15	2	9/12/2015	100	5/12/2015	33	4/20/2015	100
2016	Haig	9/13/16	1	9/13/2016	100	5/18/2016	33	4/17/2016	100
2017	Haig	9/16/17	1	9/16/2017	97	5/12/2017	33	5/21/2017	100
2018	Haig	na	na	na	na	na	na	4/27/2018	100
2014	Conrad	9/4/2014	7	9/11/2014	100	na	na	na	na
2015	Conrad	9/5/2015	9	9/12/2015	92	4/23/2015	8	4/20/2015	100
2016	Conrad	8/28/2016	31	9/12/2016	100	4/26/2016	44	4/17/2016	100
2017	Conrad	9/10/2017	42	9/17/2017	94	5/15/2017	59	5/21/2017	100
2018	Conrad	na	na	na	na	4/24/2018	56	4/26/2018	100

The Cryosphere Discuss., https://doi.org/10.5194/tc-2019-30
Manuscript under review for journal The Cryosphere
Discussion started: 18 February 2019

2015	Kokanee	8/27/2015	11	9/12/2015	100	4/20/2015	20	4/19/2015	100
2016	Kokanee	9/5/2016	23	9/13/2016	100	4/19/2016	33	4/17/2016	100
2017	Kokanee	9/19/2017	15	9/16/2017	83	4/17/2017	23	5/21/2017	100
2018	Kokanee	na	na	na	na	4/18/2018	21	4/26/2018	100

Table 3: Seasonal balance and uncertainty estimates for geodetic (geod) and glaciological mass balance (glac.) in m w.e. Kinematic GPS survey-derived corrections applied to glaciological data (surv.corr). Statistical analysis of the DEMs in snow and ice-free terrain include NMAD, median height difference, bias correction applied over the glacier ($Bias_{\Delta h}$) and mean density of Ba_{geod}. Average values exclude cases where only geodetic or glaciologic data were collected. $Bw_{geod.gl}$ is calculated using glaciological densities (Table S1), and $Bw_{geod.sc}$ is calculated using snow course data (Figure 2). Listed Bs_{geod} is derived using $Bw_{geod.sc}$, and Ba_{geod} used regional late-summer snow density (Table 5).

Year	Glacier	$Bw_{geod.gl} \pm \sigma_{geod.bw}$	$Bw_{geod.sc} \pm \sigma_{geod.bw}$	$Bs_{geod} \pm \sigma_{geod.bs}$	$Ba_{geod} \pm \sigma_{geod.ba}$	$Bw_{glac} \pm \sigma_{glac.bw}$	$Bs_{glac} \pm \sigma_{glac.bs}$	$Ba_{glac} \pm \sigma_{glac.ba}$	$Bw_{surv.corr}$	$Ba_{surv.corr}$	AAR	ELA (m)	NMAD Ba (m)	NMAD Bw (m)	Median $Ba_{\Delta h}$ (m)	$Bias_{\Delta h}$ (m)	$\bar{\rho}$ (kg m^{-3})
2018	Zillmer	1.70 ± 0.19	1.75 ± 0.20			1.65 ± 0.17			-0.15					1.4			
2018	Nordic	1.87 ± 0.26	2.07 ± 0.27			2.18 ± 0.14			-0.04					1.76			
2018	Illecillewaet	1.61 ± 0.17	1.65 ± 0.18			—			na					2.26			
2018	Haig	1.25 ± 0.15	1.31 ± 0.19			1.42 ± 0.15			na					1.83			
2018	Conrad	1.62 ± 0.21	1.84 ± 0.23			1.83 ± 0.12			0.00					2.34			
2018	Kokanee	2.07 ± 0.25	2.31 ± 0.26			2.25 ± 0.13			0.01					1.76			
2017	Zillmer	2.12 ± 0.24	2.03 ± 0.25	-2.70 ± 0.27	-0.67 ± 0.10	1.93 ± 0.26	-2.44 ± 0.35	-0.51 ± 0.23	0.15	-0.31	0.48	2440	0.6	1.83	-0.1	-0.05	729 ± 45
2017	Nordic	2.14 ± 0.29	2.18 ± 0.30	-2.77 ± 0.31	-0.59 ± 0.09	2.03 ± 0.22	-2.78 ± 0.32	-0.75 ± 0.23	-0.04	-0.10	0.39	2540	0.28	1.8	0.01	-0.09	732 ± 43
2017	Illecillewaet	1.47 ± 0.19	1.54 ± 0.20	-2.55 ± 0.27	-1.01 ± 0.18	2.00 ± 0.16	-2.84 ± 0.32	-0.84 ± 0.28	—	—	0.36	2615	0.32	2.19	0.01	0	718 ± 49
2017	Haig	1.58 ± 0.20	1.65 ± 0.23	-3.56 ± 0.31	-1.91 ± 0.21	1.50 ± 0.17	-3.43 ± 0.29	-1.93 ± 0.24	—	—	0.04	na	0.31	1.62	0.01	0.04	885 ± 10
2017	Conrad	2.10 ± 0.22	1.91 ± 0.23	-2.97 ± 0.26	-1.06 ± 0.13	2.17 ± 0.17	-3.12 ± 0.29	-0.95 ± 0.24	-0.16	-0.16	0.48	2600	0.31	2.68	0	-0.01	730 ± 45
2017	Kokanee	3.15 ± 0.32	2.86 ± 0.33	-3.14 ± 0.34	-0.28 ± 0.08	2.84 ± 0.25	-2.87 ± 0.34	-0.03 ± 0.23	0.00	0.01	0.62	2560	0.34	1.99	-0.08	-0.01	711 ± 55
2016	Zillmer	1.68 ± 0.19	1.72 ± 0.20	-2.27 ± 0.22	-0.55 ± 0.07	1.99 ± 0.23	-2.61 ± 0.33	-0.62 ± 0.24	0.02	-0.38	0.49	2410	0.21	1.76	0.01	-0.02	726 ± 46
2016	Nordic	1.79 ± 0.22	1.70 ± 0.23	-1.85 ± 0.24	-0.15 ± 0.08	1.79 ± 0.14	-1.90 ± 0.21	-0.11 ± 0.16	-0.08	0.01	0.43	2555	0.16	1.63	0	-0.04	727 ± 40
2016	Illecillewaet	1.41 ± 0.17	1.46 ± 0.18	-1.73 ± 0.18	-0.27 ± 0.05	—	—	-0.19 ± 0.28	—	—	0.60	2550	0.45	1.9	-0.01	0.05	718 ± 54
2016	Haig	1.15 ± 0.15	1.21 ± 0.17	-2.27 ± 0.20	-1.06 ± 0.11	1.34 ± 0.17	-2.49 ± 0.29	-1.15 ± 0.24	—	—	0.03	na	0.38	1.24	-0.01	-0.04	893 ± 10
2016	Conrad	1.40 ± 0.18	1.47 ± 0.19	-1.74 ± 0.20	-0.27 ± 0.06	1.88 ± 0.12	-2.08 ± 0.20	-0.20 ± 0.16	0.11	-0.13	0.55	2530	0.14	2.1	0	-0.02	734 ± 50
2016	Kokanee	1.98 ± 0.22	2.05 ± 0.23	-1.93 ± 0.23	+0.12 ± 0.05	2.07 ± 0.13	-1.94 ± 0.26	+0.13 ± 0.22	-0.05	0.12	0.72	2545	0.15	1.67	0	0	681 ± 64
2015	Zillmer	—	—	—	—	2.06 ± 0.30	-2.82 ± 0.40	-0.76 ± 0.27	0.00	-0.32	0.30	2500	—	—	—	—	—
2015	Nordic	1.74 ± 0.22	1.81 ± 0.23	-2.81 ± 0.28	-1.0 ± 0.16	1.83 ± 0.19	-3.02 ± 0.31	-1.19 ± 0.24	-0.16	0.06	0.32	2610	0.26	1.76	0	0.02	744 ± 42
2015	Illecillewaet	—	—	—	—	—	—	-1.17 ± 0.47	—	—	0.30	2600	—	—	—	—	—
2015	Haig	—	—	—	—	1.23 ± 0.25	-3.02 ± 0.25	-1.79 ± 0.25	—	—	0.00	na	—	—	—	—	—
2015	Conrad	1.65 ± 0.17	1.64 ± 0.18	-3.06 ± 0.24	-1.42 ± 0.16	1.80 ± 0.13	-3.20 ± 0.35	-1.40 ± 0.32	-0.02	-0.31	0.44	2685	0.21	2.2	-0.01	-0.03	736 ± 43
2015	Kokanee	—	—	—	—	2.18 ± 0.29	-3.38 ± 0.40	-1.20 ± 0.28	0.00	—	0.20	2680	—	—	—	—	—
All	Average	1.84 ± 0.11	1.88 ± 0.09	-2.59 ± 0.16	-0.72 ± 0.16	1.95 ± 0.08	-2.71 ± 0.13	-0.70 ± 0.15	-0.04	-0.14	0.38	2553	0.29	1.89	-0.01	-0.01	748 ± 62

Table 4: Density values used for geodetic and glaciological balance. Glaciological values are average values.

Density	Geodetic (kg m^{-3})	Glaciological (kg m^{-3})	n
ρ_{spring}	470 ± 70*	457 ± 50*	74
ρ_{snow}	590 ± 90	570 ± 20	27
ρ_{firn}	700 ± 100	703 ± 65	4
ρ_{ice}	910 ± 10	—	—

***Geodetic spring snow density (ρ_{spring}) is 440 ± 50 kg m^{-3} for Haig Glacier and glaciological is 420 ± 45 kg m^{-3} (n = 46).**

The Cryosphere Discuss., https://doi.org/10.5194/tc-2019-30
Manuscript under review for journal The Cryosphere
Discussion started: 18 February 2019

Table 5: Late-summer snow density observations from regional studies. We use 575 kg m^{-3} as our density of late-summer snow for geodetic mass balance, but also separately calculate mass balance using the average for regional studies excluding those from our study glaciers (590 kg m^{-3}).

Location	Mean ρ_{snow} (kg m^{-3})	Range ρ_{snow} (kg m^{-3})	References
South Cascade Gl., WA, USA	580	530 – 600	(Bidlake et al., 2010; Krimmel, 1996)
Juneau Icefield, AK, USA	560	540 – 580	(Miller and Pelto, 1999; Pelto and Miller, 1990)
Castle Creek Gl., BC, CA	600	—	(Beedle et al., 2014)
North Cascades, WA, USA	600	590 – 630	(Pelto and Riedel, 2001)
Haig Glacier, AB, CA	545	530 – 570	(Marshall, 2012)
Columbia Basin, BC, CA	570	535 – 615	This study

690

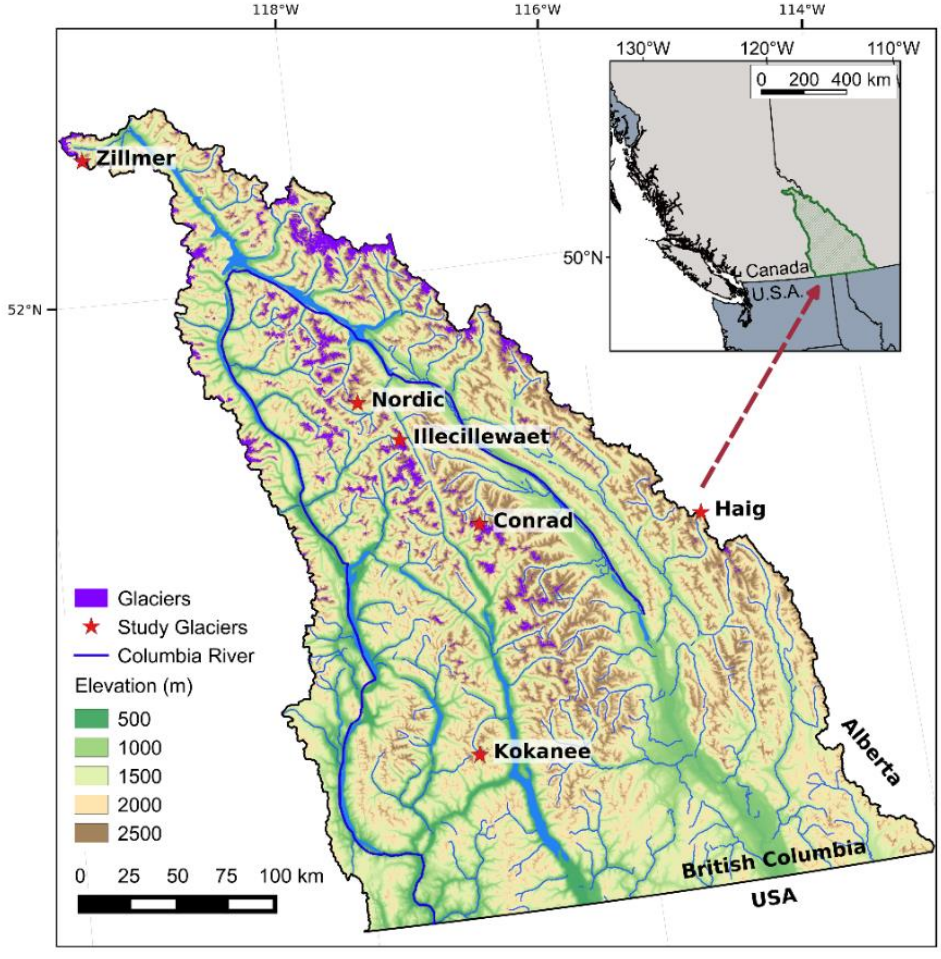

Figure 1: Map of the Canadian Columbia River Basin and locations of study sites.

The Cryosphere Discuss., https://doi.org/10.5194/tc-2019-30
Manuscript under review for journal The Cryosphere
Discussion started: 18 February 2019

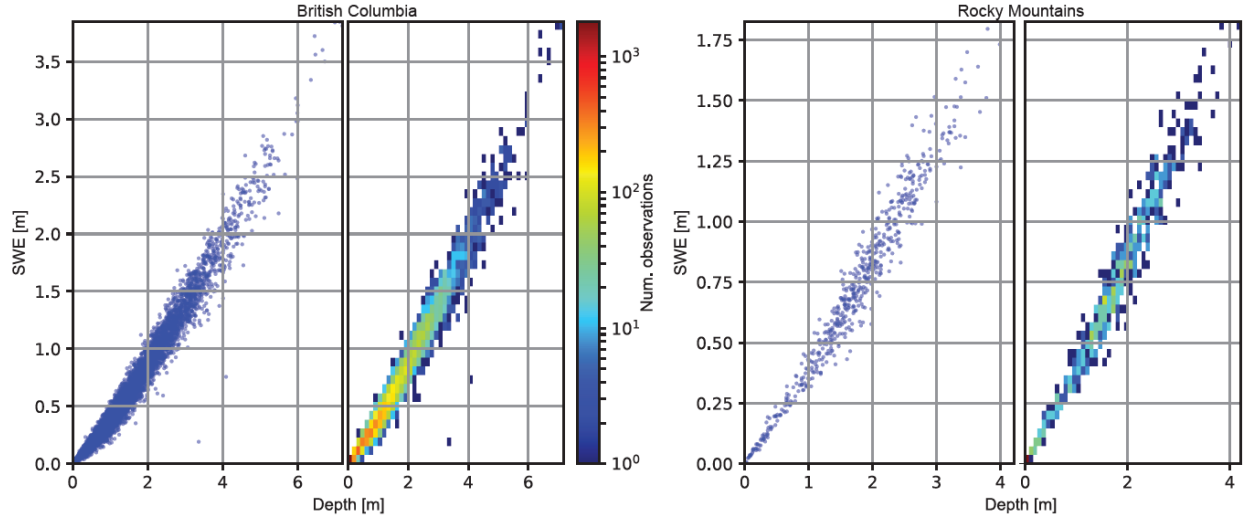

Figure 2: Snow depth versus snow water equivalent from May 1 provincial snow course data. The mean date of our spring field seasons was May 1, and so we chose May 1 BC snow course data (left) to derive a SWE/snow depth regression from which we determined the average May 1 snow density is 470 ± 70 kg m^{-3} (r^2 = 0.97, n = 10,169). For Haig Glacier, we derived a regression from only snow stations within the Rocky Mountains from Pine Pass south to derive winter density (440 ± 50 kg m^{-3} (r^2 = 0.97, n = 629)

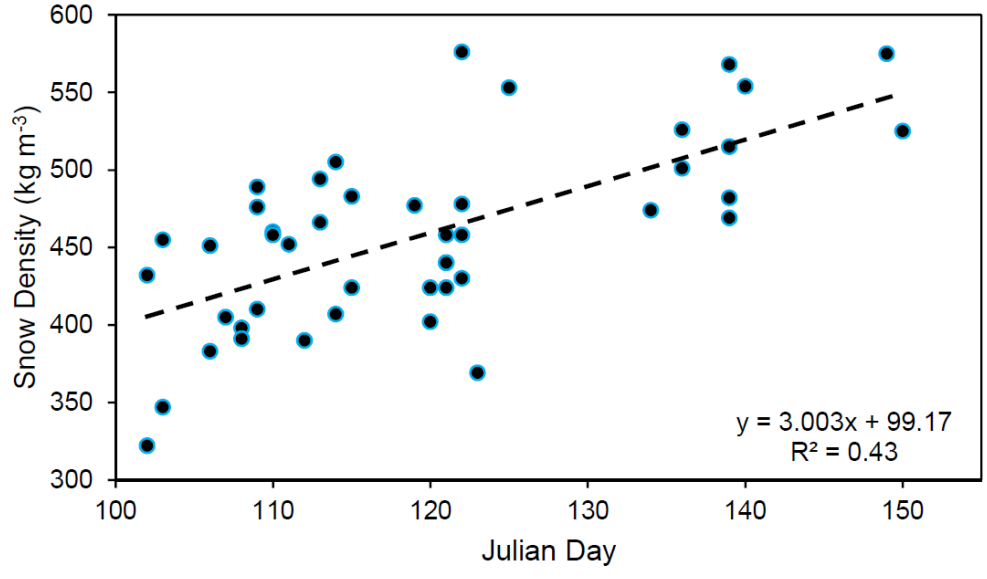

Figure 3: Snow density versus Julian day for all discrete snow pit and snow core locations (n = 46). For our glaciological density-informed estimates, we use the observed glacier-wide snow density and a linear regression of density versus day and used the slope (3.0 kg m^{-3} day^{-1} (r^2 = 0.43)) and days between the survey and the observations to adjust for change in snow density (Table S1).

The Cryosphere Discuss., https://doi.org/10.5194/tc-2019-30
Manuscript under review for journal The Cryosphere
Discussion started: 18 February 2019

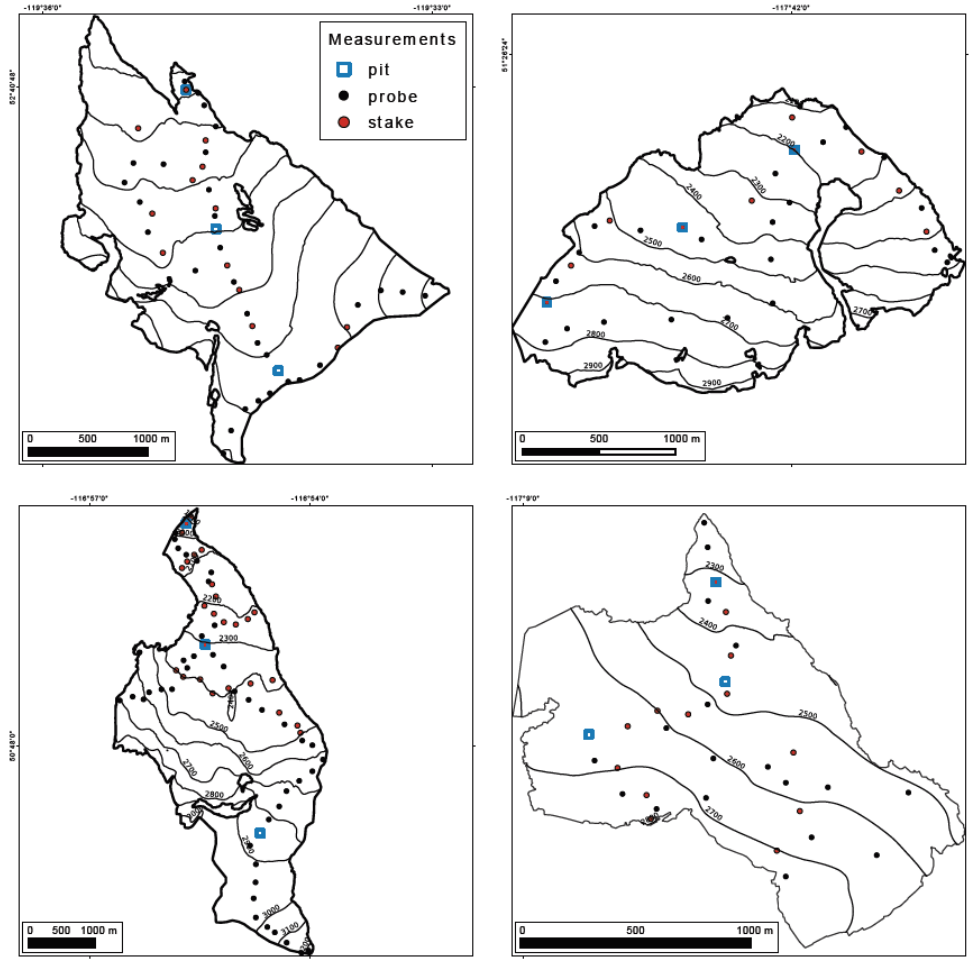

Figure 4: Measurement networks for the (clockwise from top left) Zillmer, Nordic, Kokanee, and Conrad glaciers. Snow depth measurement locations, ablation stakes, and snow pit/core locations are pictured. Refer to Marshall et al. (2014) for the Haig Glacier, and Hirose and Marshall (2013) for the Illecillewaet Glacier.

The Cryosphere Discuss., https://doi.org/10.5194/tc-2019-30
Manuscript under review for journal The Cryosphere
Discussion started: 18 February 2019

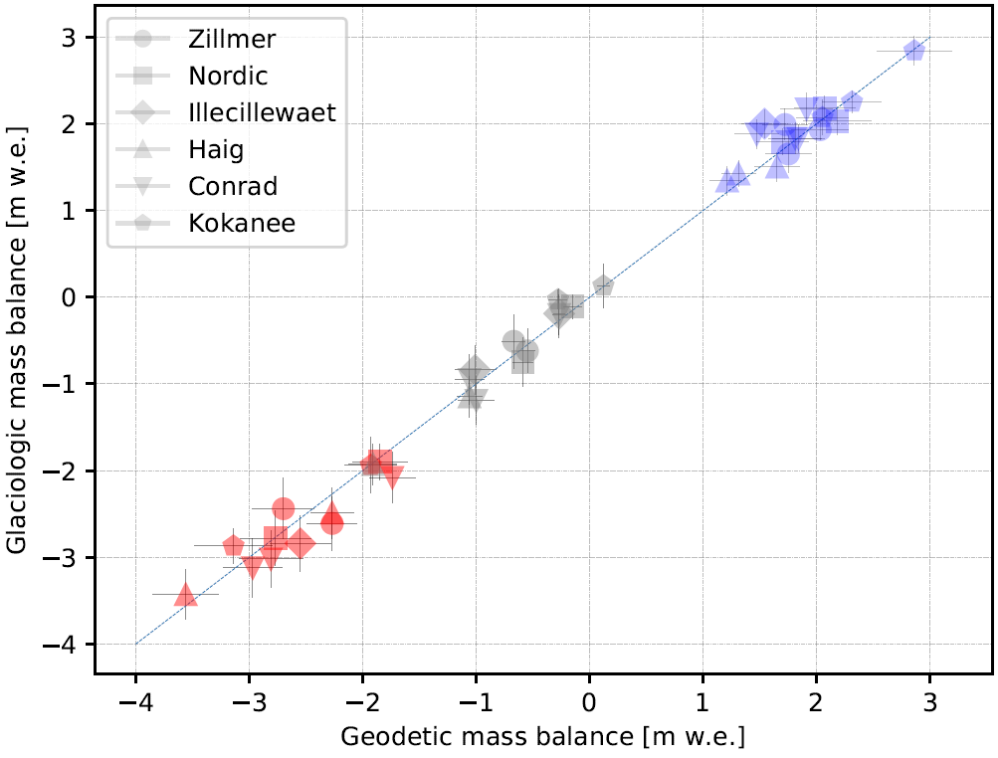

715 **Figure 5: Geodetic versus glaciological mass balance estimates for 2015 through 2018 for all six study glaciers with a one-to-one line. Winter balance (blue) covers the accumulation season from mid-September to late-April, summer balance (red) spanning the remaining months, and annual balance (grey). Errors depicted are 1σ uncertainties. Average B_{w_glac} was 4% greater than B_{w_geod}, and B_{s_glac} and B_{a_glac} were 4% greater than our geodetic estimates on average.**

The Cryosphere Discuss., https://doi.org/10.5194/tc-2019-30
Manuscript under review for journal The Cryosphere
Discussion started: 18 February 2019

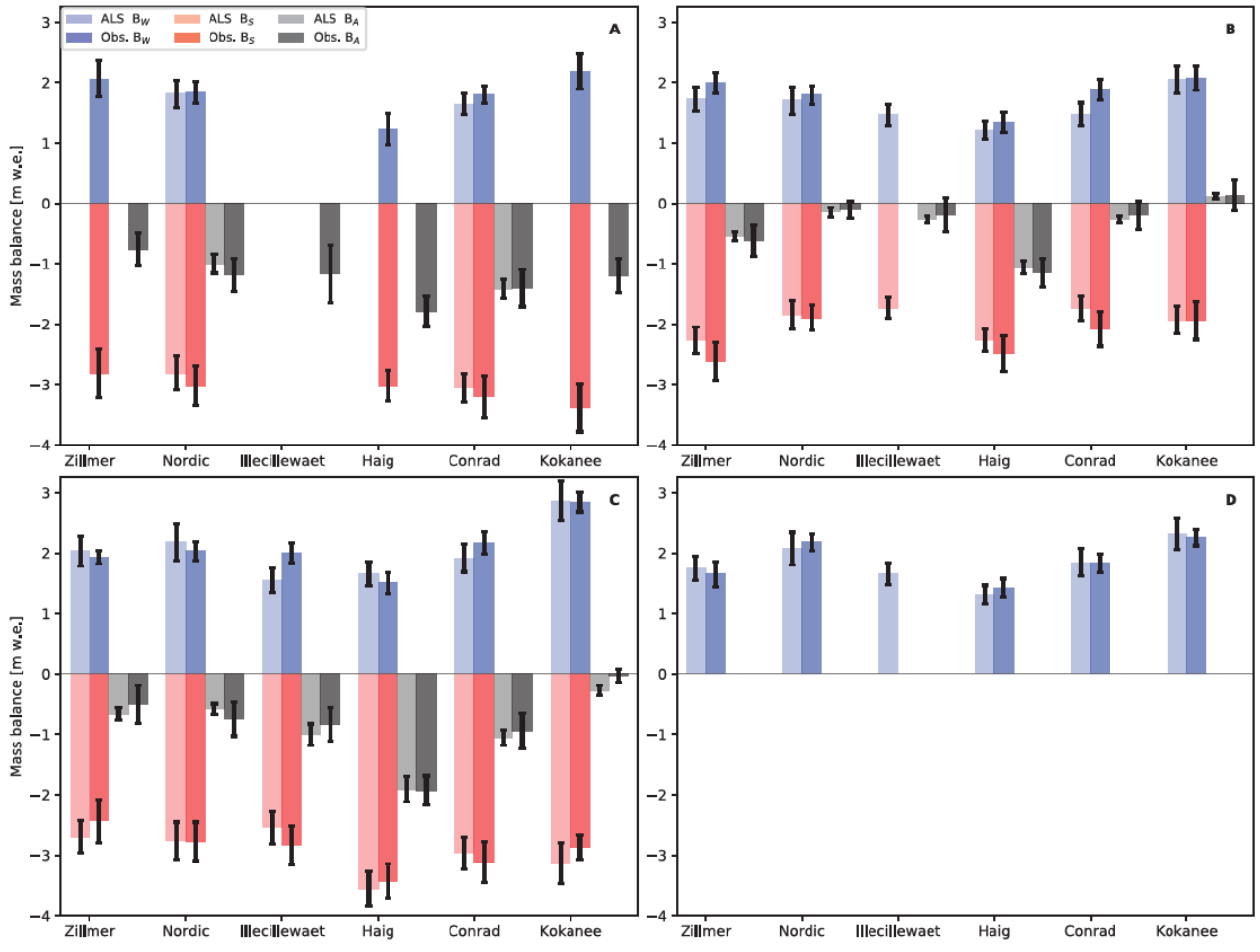

Figure 6: Seasonal and annual mass balance for all study glaciers from both geodetic and glaciological measurements for each balance year from 2014 to 2018 with 1σ uncertainties. A) 2014 to 2015 balance year, B) 2015 to 2016 balance year, C) 2016 to 2017 balance year, D) 2017 to 2018 winter balance.

The Cryosphere Discuss., https://doi.org/10.5194/tc-2019-30
Manuscript under review for journal The Cryosphere
Discussion started: 18 February 2019

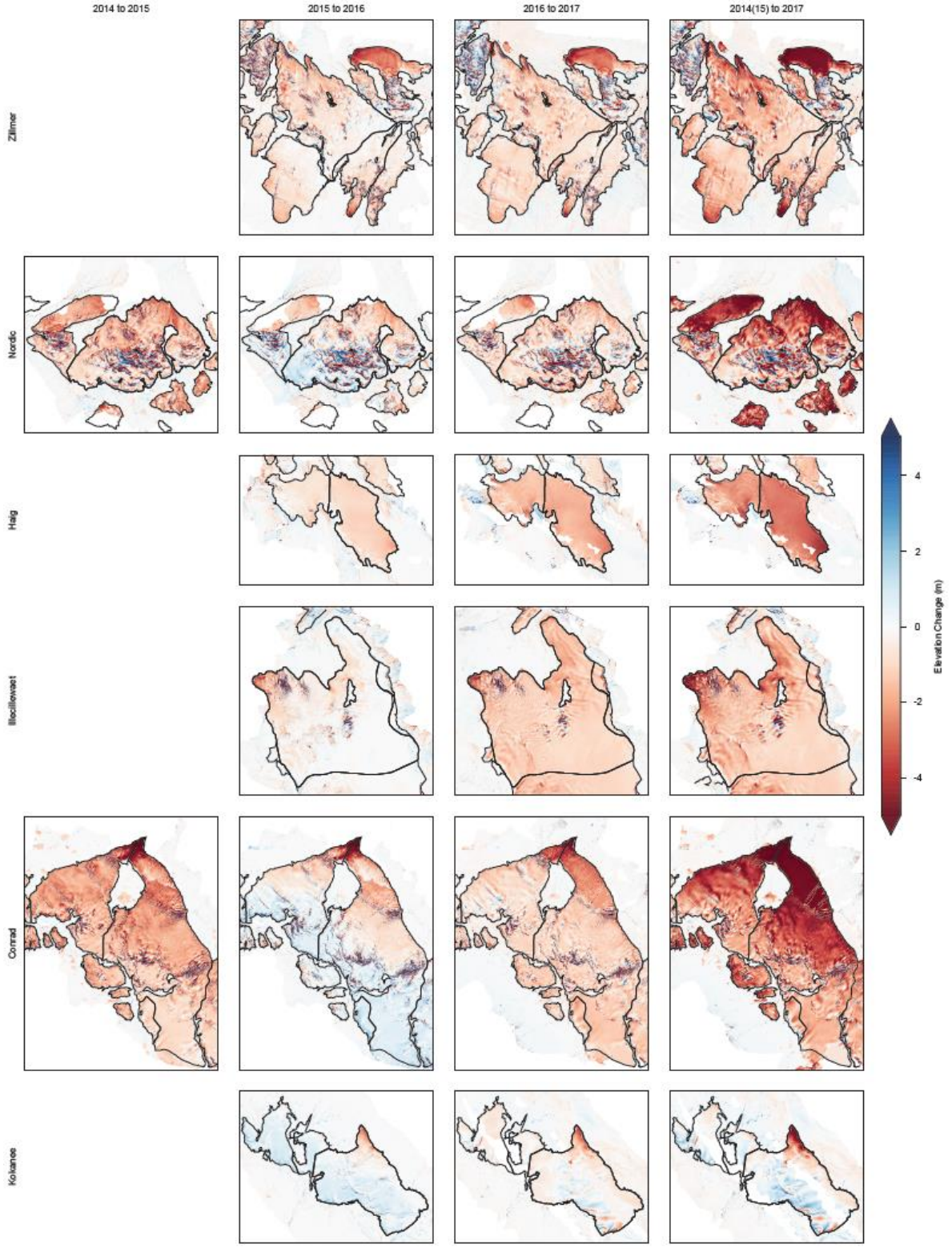

The Cryosphere Discuss., https://doi.org/10.5194/tc-2019-30
Manuscript under review for journal The Cryosphere
Discussion started: 18 February 2019

Figure 7: Surface height change for the Zillmer, Nordic, Haig, Illecillewaet, Conrad, and Kokanee glaciers from the first late-summer DEM (2014 or 2015) until late-summer 2017. Study glaciers are outlined with thick black line and other glaciers with a thin black line. Off-ice areas deemed stable terrain were used for error analysis and co-registration.

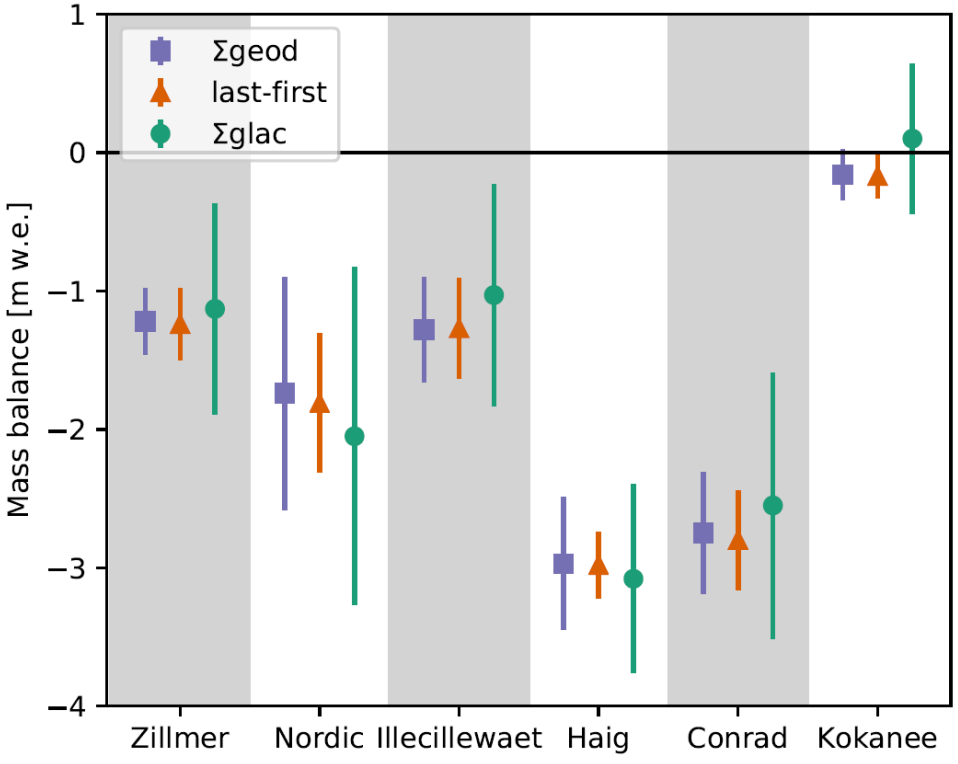

Figure 8: Summed annual mass balance from glaciological data (∑glac), geodetic data (∑geod), and last-first ΔDEM. Last-first ΔDEMs were created by differencing the first available DEM (2014 or 2015 late-summer) from the last available DEM (2017) for each site (Table 2). Errors denote 2-sigma uncertainties.